Magnesium acceptor in gallium nitride. I. Photoluminescence from Mg-doped GaN

M. A. Reshchikov, P. Ghimire, and D. O. Demchenko
Department of Physics, Virginia Commonwealth University, Richmond, Virginia 23284, USA

(Received 20 December 2017; revised manuscript received 26 April 2018; published 17 May 2018)

Defect-related photoluminescence (PL) is analyzed in detail for *n*-type, *p*-type, and semi-insulating Mg-doped GaN grown by different techniques. The ultraviolet luminescence (UVL) band is the dominant PL band in conductive *n*-type and *p*-type GaN:Mg samples grown by hydride vapor phase epitaxy (HVPE) and molecular beam epitaxy. The UVL band in undoped and Mg-doped GaN samples is attributed to the shallow Mg_{Ga} acceptor with the ionization energy of 223 meV. In semi-insulating GaN:Mg samples, very large shifts of the UVL band (up to 0.6 eV) are observed with variation of temperature or excitation intensity. The shifts are attributed to diagonal transitions, likely due to potential fluctuations or near-surface band bending. The blue luminescence (BL_{Mg}) band is observed only in GaN:Mg samples grown by HVPE or metalorganic chemical vapor deposition when the concentration of Mg exceeds $10^{19}\,cm^{-3}$. The BL_{Mg} band is attributed to electron transitions from an unknown deep donor to the shallow Mg_{Ga} acceptor. Basic properties of the observed PL are explained with a phenomenological model.

DOI: 10.1103/PhysRevB.97.205204

I. INTRODUCTION

Mg impurity in GaN is important because it is the only dopant available to produce *p*-type GaN, which is a necessary part of GaN-based electronic and optical devices. In spite of many years of research, the electronic structure of the Mg_{Ga} acceptor and the attribution of photoluminescence (PL) bands in Mg-doped GaN are still the subject of intense debates. The experimental basis for these debates is the following. Low concentrations of Mg in GaN (below $10^{17}-10^{18}\,cm^{-3}$) cause a very strong ultraviolet luminescence (UVL) band with a relatively sharp peak at 3.27 eV followed by several LO phonon replicas with decreasing intensities [1–5]. These samples are usually *n* type because of high background concentrations of shallow donors such as O_N and Si_{Ga}. *p*-type conductivity can be achieved in GaN samples grown by metalorganic chemical vapor deposition (MOCVD) doped with Mg with the concentration exceeding $10^{19}\,cm^{-3}$ after activation of the Mg acceptors by thermal annealing. However, in such samples, the blue luminescence (BL_{Mg}) band with a maximum between 2.7 and 3.0 eV is the dominant PL band [2,3,5–10]. *p*-type conductivity can also be achieved without annealing in heavily doped GaN:Mg grown by molecular beam epitaxy (MBE) [11]. In such samples, only the UVL band is observed [2,4,12,13]. The characteristic feature of the BL_{Mg} band is its significant shift to higher energies (by up to 0.2 eV) with increasing excitation intensity [2,3,5–7,9]. The BL_{Mg} band is most commonly attributed to transitions from a deep donor to the shallow Mg_{Ga} acceptor [2]. The identity of the deep donor, which is created in significant amounts in GaN:Mg samples grown by MOCVD, is also a subject of debate, and the most popular candidates for this donor are the V_NMg_{Ga} complex [6,14] and a hydrogen-related complex defect [3,15–17]. The interpretation of PL spectra is often complicated by the presence of potential fluctuations, which may cause significant shifts and distortions of PL bands in heavily Mg-doped GaN [7,18]. The UVL and BL_{Mg} bands are often confused because of these shifts and distortions. There is also no understanding of how to explain the very wide range of PL lifetimes for defect-related bands in GaN:Mg: from subnanoseconds [19] to hundreds of nanoseconds [20], to microseconds [21,22] and milliseconds [23].

First-principles calculations using density functional theory (DFT) initially predicted that Mg_{Ga} is a shallow acceptor in GaN [24,25]. However, recently Lany and Zunger [26] proposed the concept of the dual nature of acceptors in GaN. In particular, they predicted that the Mg_{Ga} acceptor in GaN has two states: a deep ground state (DGS) with a localized hole and a metastable, shallow transient state (STS) with a delocalized hole. According to their calculations, the thermodynamic $-/0$ transition level (E_A) of the STS for the Mg_{Ga} is very close to that of the DGS (0.15 and 0.18 eV, respectively), while the optical transition levels are different (about 0.15 and 0.62 eV, respectively). The thermodynamic transition level corresponds to the position of the zero-phonon line (ZPL) of the defect-related luminescence relative to the band gap ($E_A = E_g - E_{ZPL}$), whereas the optical level corresponds to the position of the PL band maximum ($\hbar\omega_{max}$), i.e., $E_0 = E_g - \hbar\omega_{max}$. According to Ref. [26], the barrier between the metastable (STS) and stable (DGS) states is $\Delta E \approx 0.02$ eV. Therefore, it is expected that in conductive *n*-type GaN doped with Mg, transitions involving the STS will dominate, because the electron-hole recombination may occur faster than the transition to the DGS state over the barrier. The STS transitions can explain the UVL band at 3.27 eV. In high-resistivity GaN samples, transitions involving the DGS will dominate, because the recombination time is expected to become longer. In this case, a luminescence with a maximum at about 2.9 eV should be observed [26]. Finally, in conductive *p*-type GaN samples, most Mg_{Ga} acceptors are expected to be in the ground state already before photoexcitation, and no PL signal corresponding to the STS should be observed. According to Ref. [26],

TABLE I. Parameters of GaN:Mg samples.

Sample	Growth method	Thickness (μm)	Conductivity type	[Mg] from SIMS (cm^{-3})	p or n (cm^{-3})
3590	HVPE	500	n	1.3×10^{17}	1.6×10^{16}[a]
3589	HVPE	500	SI	1.5×10^{18}	Undetermined
1840	HVPE	4.7	p	2×10^{19}	Undetermined
9599A	MBE	7	p	4.9×10^{19}	1.3×10^{18}[b]
9600A	MBE	7	p	2.3×10^{19}	6.1×10^{17}[b]

[a]At $T = 100$ K.
[b]At $T = 295$ K.

this theoretical model well explains early experimental results of Monemar *et al.* [1], where two Mg-related acceptors have been suggested: the A1 acceptor responsible for the 3.27 eV peak and the A2 acceptor responsible for the broader band at 3.15 eV. However, later Monemar *et al.* [3] concluded that only the 3.27 eV is related to an isolated Mg_{Ga} acceptor, while the 3.15 eV band is caused by the same defect perturbed by a nearby basal plane stacking fault.

In partial accord with Lany and Zunger [26], other groups, employing hybrid density functional calculations, have found that the hole bound to the Mg_{Ga} acceptor in the ground state is highly localized; however, they did not confirm the existence of the shallow (STS) state [27,28]. In these calculations, the values of $E_A = 0.26$ eV [27] or $E_A = 0.38$ eV [28] and $E_0 = 0.54$ eV [27] were obtained for the Mg_{Ga} acceptor. In relation to experiments, the $E_0 = 0.54$ eV value was associated with the BL_{Mg} band observed at 2.7–2.9 eV in GaN heavily doped with Mg, while the 3.27 eV band was attributed to the Mg_{Ga}-H_i complex [27]. Although it may appear that the calculations carried out in Refs. [26–28] agree with experiments, careful analysis of the experimental data reveals multiple inconsistencies, which are discussed in this work.

In this paper, we analyze in detail experimental results obtained from n-type, p-type, and semi-insulating GaN:Mg samples grown by different techniques. The results are explained quantitatively with a simple phenomenological model. In the follow-up paper [29], we present results of first-principles calculations that resolve the controversy between theory and experiment.

II. EXPERIMENTAL DETAILS

Mg-doped GaN samples grown by different techniques have been studied. Five samples with parameters listed in Table I were selected for more detailed analysis. Freestanding GaN samples 3589 and 3590 were grown at Kyma Technologies, Inc., by hydride vapor phase epitaxy (HVPE). The top surface was treated with chemical-mechanical polishing. Sample 3590 is n type, with a concentration of free electrons of 1.6×10^{16} cm^{-3} at 100 K, as obtained from time-resolved PL by using electron capture coefficients found from analysis of a large number of GaN samples [30]. The conductivity type in semi-insulating (SI) sample 3589 could not be determined from electrical measurements. Sample 1840 from Nitride Crystals, Inc., is a 1-μm-thick Mg-doped GaN grown on 3.7-μm-thick undoped GaN on sapphire substrate. The concentration of holes in the top GaN:Mg layer of this sample could not be established with the Hall effect method because of stronger n-type conductivity in the 3.7-μm-thick n-type GaN buffer layer. Samples 9599A and 9600A were grown on sapphire substrate by MBE at Paul-Drude Institute in Berlin, Germany. The preliminary results of PL characterization for these two samples are published in Refs. [31,32]. These MBE-grown samples are nonuniform and exhibit two sharply defined regions with very different properties: a region where the UVL band intensity does not change much with increasing temperature from 20 to 300 K (group A samples) and a region where PL demonstrates abrupt and tunable thermal quenching (group B samples). The behavior of Mg-related PL was explained only for group B samples in Ref. [31]. In the present work, we study in detail group A samples and explain their PL behavior. The p-type conductivity for samples 1840, 9599A, and 9600A was confirmed by PL measurements as will be explained in Sec. III B and the Appendix.

Steady-state PL was excited with an unfocused He-Cd laser (30 mW, 325 nm), dispersed by a 1200 rules/mm grating in a 0.3 m monochromator and detected by a cooled photomultiplier tube. Calibrated neutral-density filters were used to attenuate the excitation power density (P_{exc}) over the range 2×10^{-8} to 0.3 W/cm^2. Power density up to 100 W/cm^2 was achieved by focusing the laser beam. Time-resolved PL was excited with a pulsed nitrogen laser (pulses with duration of 1 ns, repetition frequency of 6 Hz, and photon energy of 3.68 eV) and analyzed with an oscilloscope. A closed-cycle optical cryostat was used for temperatures between 15 and 320 K, and a high-temperature cryostat (model VPF700 from Janis Research Company) was used for temperatures between 150 and 500 K. All of the samples were studied under identical conditions, and the PL spectra were corrected for the response of the optical system.

The quantum efficiency of PL is defined as $\eta = I^{PL}/G$, where I^{PL} is the PL intensity (in photons per second per cubic centimeter) and G is the electron-hole generation rate in the region from which the PL originates. For samples with very high efficiency (such as sample 3590), the absolute internal quantum efficiency of PL could be determined from a quantitative description of the PL quenching and concurrent rise of other PL bands by using a method explained in detail in Refs. [33,34]. Samples with η approaching unity were used as calibrated samples. For samples with low efficiency of PL, this method could not be applied. In this case, to estimate the absolute internal quantum efficiency, we compared the integrated intensity of a particular PL band with that from a calibrated GaN sample.

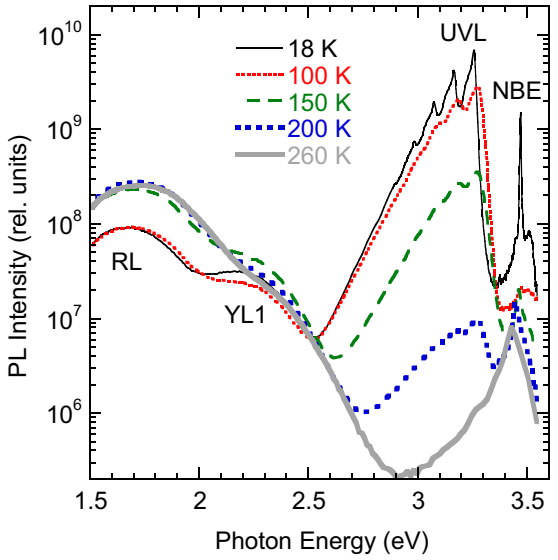

FIG. 1. Evolution of the PL spectrum with temperature for HVPE GaN:Mg sample 3590.

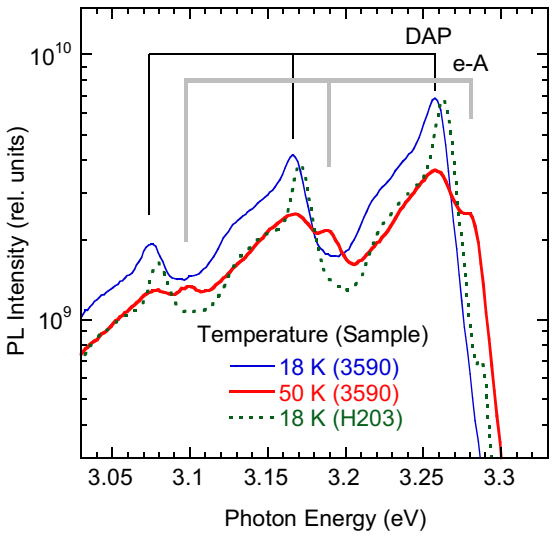

FIG. 2. The UVL band in GaN:Mg (sample 3590) at 18 and 50 K and from the undoped GaN sample (H203) at 18 K, all excited with $P_{exc} = 0.008\,W/cm^2$. The UVL band at $T = 18$ K includes the ZPL at 3.253 eV (attributed to DAP-type transitions involving a shallow donor and the shallow Mg_{Ga} acceptor) and a set of LO phonon replicas at distances multiples of 91.5 meV from the main peak. At 50 K, a series of (e-A)-type transitions appears, which correspond to electron transitions from the conduction band to the same shallow acceptor. The spectrum from sample H203 is shifted by 5 meV to lower energies to compensate strain-related blueshift in a relatively thin GaN layer on a sapphire substrate, and its intensity is multiplied by a factor of 10 to match the peak intensity of sample 3590.

III. RESULTS

A. Conductive *n*-type GaN:Mg grown by HVPE

Figure 1 shows the PL spectrum from *n*-type, conductive GaN:Mg sample with low concentration of Mg. The near-band-edge (NBE) emission contains a sharp peak at 3.471 eV, which is attributed to an exciton bound to a neutral shallow donor in stress-free GaN. A weaker peak at 3.466 eV is assigned to an exciton bound to the Mg_{Ga} acceptor [3]. Its relative intensity increases with the excitation intensity due to increasing population of the Mg_{Ga} acceptors with holes in *n*-type GaN. We did not observe the 3.455 eV line attributed to an exciton bound to the Mg_{Ga} acceptor perturbed by a nearby basal plane stacking fault [3].

In the spectral region containing PL from defects, three bands can be resolved: the UVL band with a maximum at 3.26 eV, the yellow luminescence (YL1) band with a maximum at 2.20 eV, and the red luminescence (RL) band with a maximum at 1.67 eV at 18 K. The strongest peak of the UVL band shifts from 3.253 to 3.263 eV with increasing P_{exc} from 3×10^{-5} to $0.2\,W/cm^2$. It is followed by a few LO phonon replicas. The UVL and YL1 bands are identical to those in undoped GaN [35]. The origin of YL1 and RL bands is beyond the scope of this work.

With increasing temperature, the intensity of the donor-acceptor-pair (DAP) peaks of the UVL band gradually decreases, and these peaks are replaced with very similar in shape but blueshifted free electron-to-acceptor (e-A) peaks with the ZPL at 3.280 eV at $T = 50$ K (Fig. 2). The shape of the band is very similar to the UVL band shape in undoped GaN (Fig. 2). The small redshift and broadening of peaks in GaN:Mg can be caused by weak potential fluctuations, which are negligible in the undoped GaN sample. The quantum efficiency of the UVL band, as determined from comparison with calibrated samples [34], is about 20% for the GaN:Mg sample and 2% for the undoped GaN sample. From the analysis of a large number of undoped and Mg-doped GaN samples grown by HVPE, it was established that the quantum efficiency of the UVL band increases linearly with the concentration of the shallow acceptors up to about $10^{16}\,cm^{-3}$ and saturates at higher concentrations [35].

The striking similarity of the UVL band shapes in undoped and Mg-doped GaN samples points to the same origin (Mg_{Ga}) of the shallow acceptors in these samples. The transition level $-/0$ of this defect is located at 223 ± 3 meV above the valence band maximum, the same value for undoped and Mg-doped GaN [36]. This estimate is made from the position of the e-A ZPL (3.280 eV) and the band gap of GaN (3.503 eV) at temperatures below 50 K. Earlier, the value of 224 meV was found for the Mg_{Ga} acceptor in GaN implanted with Mg [37]. In undoped GaN samples, the Mg_{Ga} defect with low concentration is expected from contamination of the Ga source with Mg. The concentrations of Mg lower than $10^{15}\,cm^{-3}$ are below detection limit of the secondary ion mass spectrometry (SIMS), yet they cause a relatively strong UVL band due to the large hole-capture coefficient of the shallow acceptor [35]. Note that other previously suggested candidates for the shallow acceptor in undoped GaN, such as Si_N and C_N defects [2], should be discarded. Modern first-principles calculations predict that the C_N and Si_N are deep acceptors with the $-/0$ transition level at 0.9 eV and 2.05 eV, respectively, above the valence band [38,39].

The integrated intensity of the UVL band remains nearly unchanged up to 130 K. At higher temperatures, the UVL band is quenched and disappears at 260 K (Figs. 1 and 3).

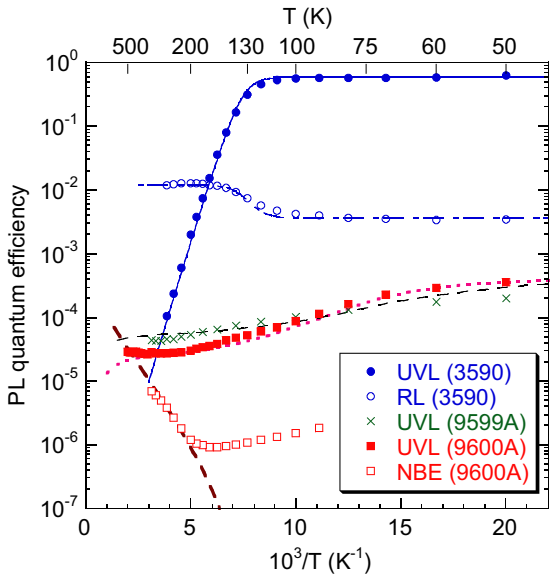

FIG. 3. Temperature dependence of PL quantum efficiency for selected PL bands in GaN:Mg samples. The solid line for sample 3590 is calculated using Eqs. (1) and (2) with the following parameters: $\eta_0 = 0.6$, $\tau_0 = 20\ \mu$s, $C_{pA} = 0.5 \times 10^{-6}\,\mathrm{cm}^3/\mathrm{s}$, $N_v = 3.2 \times 10^{15} T^{3/2}\,\mathrm{cm}^{-3}$, $E_A = 185$ meV. Other lines are from numerical solutions of Eqs (A1)–(A9) in the Appendix with parameters given in Table II.

The temperature dependence of the quantum efficiency of the UVL band, $\eta(T)$, can be fitted with the following equation obtained from the solution of rate equations for competing electron-hole recombination flows through defects in an n-type semiconductor [34,40]:

$$\eta(T) = \frac{\eta_0}{1 + C \exp\left(-\frac{E_A}{kT}\right)}. \quad (1)$$

Here, η_0 is the PL quantum efficiency in the limit of low temperatures, E_A is the activation energy of thermal quenching, and k is Boltzmann's constant. The quenching of the UVL band above 130 K is explained by thermal emission of holes from the Mg_{Ga} acceptor to the valence band. In this case, E_A is the ionization energy of the acceptor and

$$C = (1 - \eta_0)\tau_0 C_{pA} N_v g^{-1}, \quad (2)$$

where C_{pA} is the hole-capture coefficient for the acceptor, g is the degeneracy of the energy level, N_v is the effective density of states in the valence band, and τ_0 is the lifetime of the UVL band at temperatures just before its quenching.

The value of $\tau_0 = 20\ \mu$s was found from time-resolved PL measurements. The characteristic time of the thermal emission of holes from the acceptor A to the valence band, τ_{therm}, can be defined as

$$\tau_{\mathrm{therm}} = \frac{g \exp\left(\frac{E_A}{kT}\right)}{(1 - \eta_0) C_{pA} N_v}. \quad (3)$$

At $\tau_{\mathrm{therm}} \gg \tau_0$, PL intensity is independent of temperature, and at $\tau_{\mathrm{therm}} \ll \tau_0$, an exponential decrease is observed. The transition from the temperature-independent region of the $\eta(T)$ dependence to the exponential decrease occurs at the characteristic temperature $T_A \approx 135$ K (Fig. 3), which can be found from the condition $\tau_{\mathrm{therm}}(T_A) = \tau_0$.

It is important to note that no defect-related bands, other than the UVL band, could be found at photon energies between 2.7 and 3.3 eV (Fig. 1). Simultaneously with the quenching of the UVL band, the intensities of the YL1 and RL bands increase by a factor of 3 with increasing temperature from 100 to 160 K (Figs. 1 and 3). This is an indication of a very high internal quantum efficiency of the UVL band. The rise of the YL1 and RL bands [41] is explained by redistribution of holes thermally emitted from the Mg_{Ga} acceptor to the valence band between all recombination channels. From the value of this rise we estimate [34] that $\eta_0 = 0.6$–0.7 for the UVL band. Independently, using comparison with calibrated GaN samples [34,35], η for the UVL band is estimated as 20% at the lowest temperature. The former should be considered as a more accurate value because the *internal* quantum efficiency of PL can be reliably determined when it is very high, by using a simple phenomenological model [40]. On the other hand, comparison with calibrated samples can cause an error by up to a factor of 3 due to different light extraction efficiencies in different GaN samples [35].

The concentration of Mg in this sample was determined from the SIMS analysis as $1.3 \times 10^{17}\ \mathrm{cm}^{-3}$, and the concentration of free electrons at $T = 100$ K was found to be $1.6 \times 10^{16}\ \mathrm{cm}^{-3}$ from time-resolved PL measurements by a method described in Refs. [30,42]. The thermal quenching of the UVL band above ~100 K with the activation energy of ~0.2 eV is a clear fingerprint of the n-type conductivity, as explained in the Appendix. Observation of such $I^{PL}(T)$ dependence in GaN:Mg can serve as a proof of n-type conductivity when the Hall effect measurements are inconclusive or cannot be done. A very different temperature behavior is observed for the UVL band in conductive p-type GaN.

B. Conductive *p*-type GaN:Mg grown by MBE

The evolution of the PL spectrum with temperature for p-type GaN:Mg grown by MBE is shown in Fig. 4. At the lowest temperature, the UVL band has the usual shape with the ZPL at 3.27 eV, yet the peaks are noticeably broadened. The excitonic peak (labeled NBE) is much weaker, which is typical for p-type GaN:Mg samples. The second defect-related band, which has a maximum at 2.38 eV, is identified as the GL2 band and has been attributed to the nitrogen vacancy (V_N) defect [32]. After a laser pulse in time-resolved PL measurements, the UVL intensity decays very fast (faster than time resolution of our system, which is 10 ns).

With increasing temperature from 50 to 150–200 K, the intensity of the UVL band decreases as $I^{PL} \propto \exp(E_D/kT)$ with $E_D \approx 20$ meV (Figs. 3 and 4). This decrease is explained by thermal emission of electrons from shallow donors to the conduction band and their recapture by nonradiative centers. The experimentally observed $I^{PL}(T)$ dependencies for p-type, MBE-grown GaN:Mg samples can be explained in a wide range of temperatures (between 18 and 300 K) only on the assumption that the dominant nonradiative center is a deep acceptor with high-capture cross sections for both electrons and holes (see Appendix). Electrons in p-type GaN are minority carriers, and several recombination channels compete

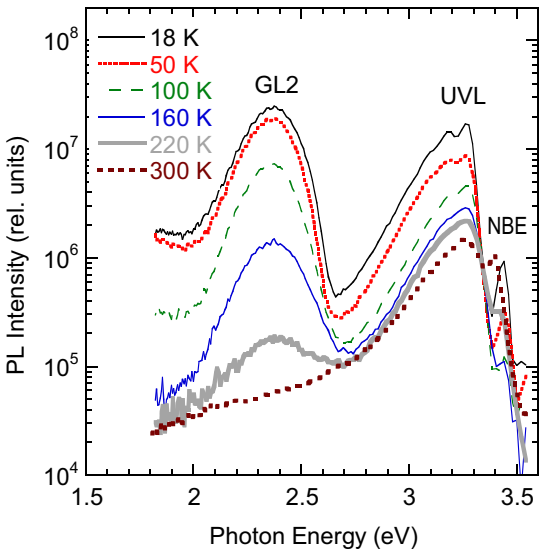

FIG. 4. Evolution of the PL spectrum with temperature for MBE GaN:Mg sample 9599A. $P_{exc} = 0.001\ W/cm^2$.

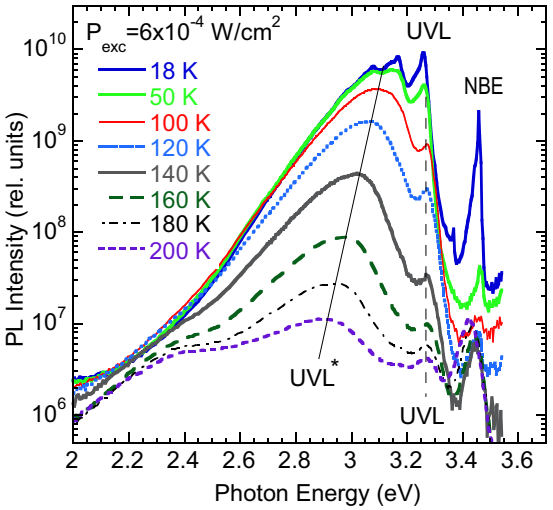

FIG. 5. Evolution of the PL spectrum with temperature for HVPE GaN:Mg, sample 3589. The UVL band does not shift, while the UVL* band monotonically shifts to lower energies with increasing temperature.

for their capture. The activation energy of PL quenching in this case is the ionization energy of the shallow donor. At temperatures between 200 and 500 K, the UVL band intensity is nearly independent of temperature (Fig. 3), in contrast to n-type GaN:Mg. Such $I^{PL}(T)$ dependence proves that the MBE-grown GaN:Mg samples are p type and the Fermi level is close to the shallow Mg_{Ga} level. Indeed, the concentration of holes bound to the Mg_{Ga} acceptor, N_A^0, is of the same order of magnitude as the concentration of Mg (more than $10^{19}\ cm^{-3}$) in the entire range of temperatures in our experiment. The thermal emission of the holes to the valence band depletes the acceptors of bound holes by less than 10% up to room temperature and does not play any significant role in the recombination statistics, as shown in the Appendix. Contrary to p-type GaN:Mg, N_A^0 in n-type GaN:Mg is very low at low P_{exc}, and it decreases with temperature above critical temperature $T_A \approx 130$ K with the activation energy equal to the ionization energy of the Mg_{Ga} acceptor.

Another interesting feature in the $I^{PL}(T)$ dependence for p-type GaN samples is the rise of NBE emission intensity with temperature above ~200 K (Figs. 3 and 4). This rise is explained by increasing concentration of holes in the valence band. The concentration of free holes increases as $p \propto \exp(-E_A/kT)$ (see Appendix), and the NBE intensity at these temperatures is proportional to the product of p and n, where n is independent of temperature. Unlike the stepwise rise of PL in n-type GaN:Mg (Fig. 3), this exponential rise cannot be explained by enhancement of all PL bands when one, very efficient recombination channel is quenched. Indeed, the quantum efficiency of PL in conductive p-type GaN is very low, and only the NBE intensity is rising with temperature at $T > 200$ K. We observed similar rise of the NBE band intensity in other conductive p-type GaN:Mg samples grown by different techniques and did not observe such behavior in semi-insulating or conductive n-type GaN samples.

C. Semi-insulating GaN:Mg grown by HVPE

Evolution of the PL spectrum with temperature in semi-insulating GaN:Mg is shown in Fig. 5. At $T = 18$ K, the UVL band with the ZPL at 3.26 eV is the dominant feature in the spectrum. Its quantum efficiency is very high, about 20% from comparison with calibrated samples. The shape of the UVL band at 18–50 K is distorted by another, structureless band, which has a maximum at about 3.1 eV at these temperatures (Fig. 5). We call this band the UVL* band and below provide the evidence that this is the Mg_{Ga}-related UVL band, which originates from semi-insulating regions of the nonuniform sample and whose shape and position are distorted by diagonal transitions due to either potential fluctuations or near surface band bending. With increasing temperature, the UVL* band is quenched and disappears under background signal at $T >$ 250 K. Interestingly, the quenching of the "normal" UVL band stops at $T = 200$ K (Fig. 5), and its intensity remains unchanged at higher temperatures, at least up to 320 K (not shown). The intensity of the NBE band reaches its minimum at $T = 140$ K and gradually increases at higher temperatures (totally, by a factor of 5 at $T = 320$ K). The rise of the NBE band and the independence of the UVL band intensity on temperature above 200 K indicate that these bands originate from conductive p-type regions of the nonuniform sample (Sec. III B).

Figure 6 shows PL spectra at 100 K at different excitation intensities, where the UVL and UVL* bands can be clearly distinguished. To better resolve these two bands, we performed deconvolution of PL spectra at various excitation intensities and temperatures. In this deconvolution, the shape of the "pure" UVL band at each temperature was taken from measurements at very high excitation intensity ($12\ W/cm^2$) where no traces of the UVL* band could be noticed and the shape of the UVL band was similar to that in n-type GaN:Mg. The "pure" UVL band was subtracted from PL spectra measured at much lower excitation intensities. The remaining spectrum revealed the

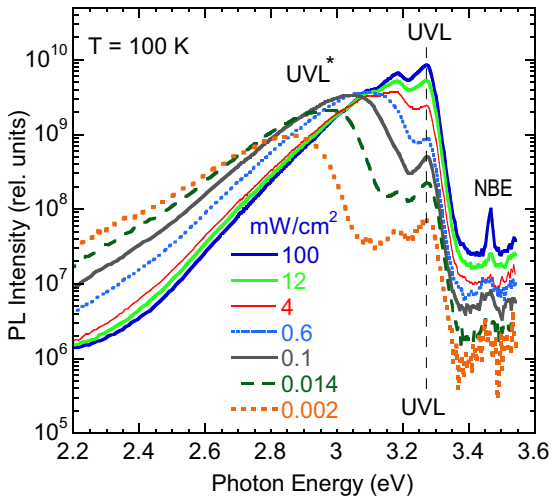

FIG. 6. PL spectra from GaN:Mg, sample 3589, at $T = 100$ K and different excitation power densities (indicated with numbers in mW/cm^2). The PL intensity is divided by the excitation intensity for convenience of comparison. The UVL band does not shift, while the UVL* band shifts monotonically to higher energies with increasing excitation intensity.

UVL* band with a characteristic asymmetric shape. The UVL* band shape was simulated with a formula obtained from a one-dimensional configuration coordinate model to determine the position of the band maximum, $\hbar\omega_{\max}$. We estimate the error in $\hbar\omega_{\max}$ as about ± 0.05 eV for $P_{\rm exc} < 0.1$ W/cm^2. More details about the deconvolution and its examples can be found in Ref. [43].

With increasing excitation intensity, the UVL band does not change its shape and position, whereas the UVL* band shifts markedly to higher energies and eventually merges with the UVL band (Fig. 6). Figure 7 shows the temperature dependence of the PL band maxima for the UVL and UVL* bands at different excitation intensities. The shift of the UVL band

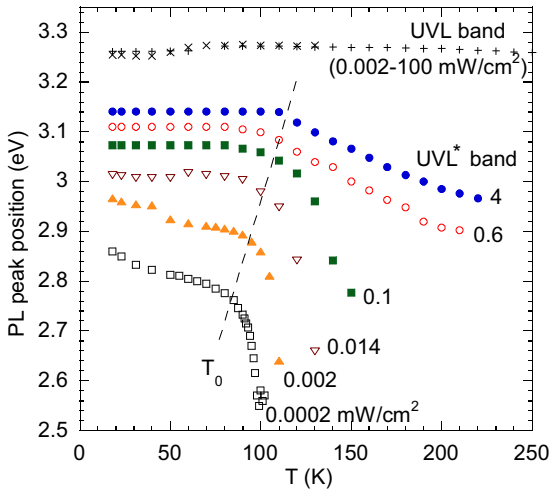

FIG. 7. Peak position of the UVL and UVL* bands in GaN:Mg (sample 3589) as a function of temperature at different $P_{\rm exc}$ (indicated with numbers in mW/cm^2). T_0 is the characteristic temperature at which the rate of the shift abruptly changes.

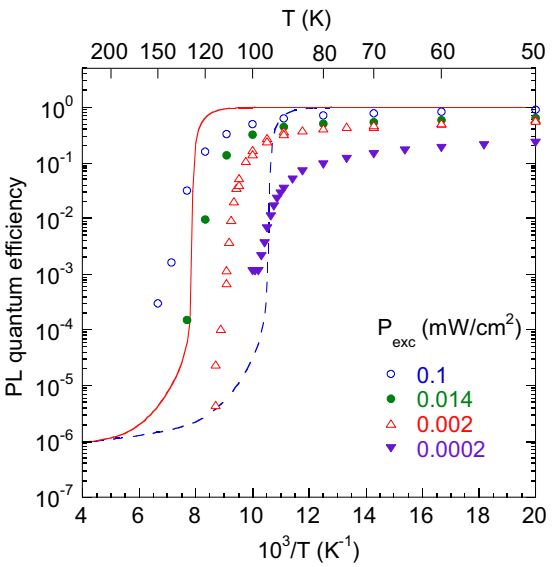

FIG. 8. Temperature dependence of the UVL* quantum efficiency at different excitation intensities for sample 3589. The symbols are experimental data (multiplied by a factor of 5 for convenience of comparison). The lines are from the numerical solution of Eqs. (A1)–(A9) in the Appendix with the following parameters: $N_A = 1.5 \times 10^{18}$, $N_S = 8 \times 10^{17}$, $N_D = 5 \times 10^{17}$ (all in cm^{-3}); $C_{pA} = 5 \times 10^{-7}$, $C_{pS} = 1 \times 10^{-10}$, $C_{nA} = 3.2 \times 10^{-12}$, $C_{DA} = 1 \times 10^{-13}$, $C_{nD} = 1 \times 10^{-8}$, $C_{nS} = 1 \times 10^{-6}$ (all in cm^3/s); $E_D = 20$ meV, $E_A = 185$ meV; $P_{\rm exc} = 0.1$ mW/cm^2 (solid line), and 0.0002 mW/cm^2 (dashed line).

maximum is negligible when the temperature is varied between 18 and 250 K at fixed excitation intensity, or when the excitation power density increases from 2×10^{-6} to 0.1 W/cm^2 at fixed temperature. The shift of the UVL* band is very large, both with temperature and excitation intensity (between 2×10^{-7} and 4×10^{-3} W/cm^2). Interestingly, the rate of the shift with temperature changes at some critical temperature T_0: at $T < T_0$, the red shift of the UVL* band is moderate, while at $T > T_0$, the shift of the UVL* band becomes enormous, especially for very low excitation intensities (Fig. 7). Note that T_0 increases with increasing excitation intensity (Fig. 7). Simultaneously with a very large shift, the abrupt thermal quenching of the UVL* band is observed at $T \approx T_0$ (Fig. 8). We observed abrupt and tunable thermal quenching for all major PL bands in this sample: the NBE, UVL, and UVL*, similarly to the case of GaN:Zn [34]. Below the effect of abrupt and tunable quenching of PL is briefly explained.

The abrupt and tunable quenching of PL can be qualitatively understood with the help of the schematics shown in Fig. 9. Detailed quantitative analysis is given in the Appendix. This mechanism of PL quenching requires at least two recombination channels: radiative recombination via the Mg_{Ga} acceptor A and a competing nonradiative recombination via a deep donor S. The quenching mechanism hinges on the balance of radiative/nonradiative rates between these channels. The hole capture coefficient C_{pA} for the Mg_{Ga} is found from quenching of steady state PL in n-type GaN (Sec. III A), while other parameters are varied within reasonable range to obtain agreement with observed behavior of PL (see Appendix for details).

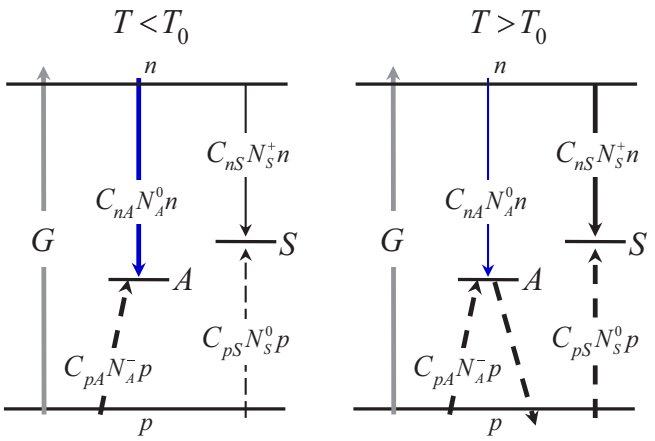

FIG. 9. Schematics of transitions explaining abrupt and tunable quenching of PL. Radiative recombination channel A competes with nonradiative recombination channel S for nonequilibrium electrons and holes generated with rate G by a laser. The thick and thin lines indicate high and low transition rates, respectively. The solid and dashed lines show the electron and hole transitions, respectively. The C_{ij} are capture coefficients described in the text. The nonradiative recombination channel is partially blocked at $T < T_0$, because deep donors S are saturated with electrons (small N_S^+) due to large C_{nS}. The acceptor A is not saturated with holes, because it is partially compensated by shallow donors. The PL efficiency is very high. At $T > T_0$, thermal emission of holes from acceptor A to the valence band becomes very efficient. These holes unblock the nonradiative channel, and PL is abruptly quenched in a narrow range of temperatures. The T_0 increases with G, because higher temperature is needed to satisfy parity of thermally emitted and photogenerated holes in the valence band.

In the dark, due to the presence of shallow and deep donors, Mg_{Ga} acceptors are partially filled with electrons. Under continuous illumination, photogenerated holes are captured very efficiently by negatively charged acceptors, while electrons are predominantly captured by deep donors. This happens because the capture coefficients C_{pA} for holes on Mg_{Ga} and C_{nS} for electrons on the deep donor are both large ($\sim 10^{-6}$ cm^3/s), while other capture coefficients are much smaller. As a result, in steady-state conditions, deep donors become saturated with electrons, and acceptors are almost (due to remaining compensation by shallow donors) saturated with holes. The saturation of the S centers with electrons, i.e., the deficit of positively charged deep donors ($N_S^+ = 2 \times 10^{-6} N_S^0$ for parameters used in Fig. 8), leads to a blockade of the nonradiative recombination channel and consequently to a significant increase in quantum efficiency of PL associated with the Mg_{Ga} acceptor.

With increasing temperature, thermal emission of holes from the Mg_{Ga} acceptors leads to increased nonequilibrium concentration of free holes and thus to increased hole capture rate by nonradiative deep donors. The increased hole-capture rate opens up the nonradiative channel, leading to abrupt drop in PL intensity at critical temperature T_0. The physical meaning of the T_0 is the critical temperature at which the concentration of thermally emitted holes in the valence band is approximately equal to the concentration of photogenerated holes. Therefore, T_0 increases with increasing electron-hole generation rate; i.e., the PL quenching is tunable by excitation intensity.

The coexistence of the UVL and UVL* bands in the same sample can be explained if we assume that the GaN:Mg layer is nonuniform: the UVL* band originates from semi-insulating regions where potential changes are significant, whereas the UVL and NBE bands are observed from conductive, p-type regions with flat potential. Such attributions are supported by the following experimental facts: (i) only the UVL* band demonstrates large shifts with increasing excitation intensity or temperature, while potential fluctuations or near-surface band bending are expected to cause similar shifts for different PL bands; (ii) the intensity of the NBE band increases with temperature and the intensity of the UVL band has very weak temperature dependence at $T > 150$ K, which is typical for conductive, p-type GaN samples (see Sec. III B and Appendix).

We observed the coexistence of the "moving" and "fixed" PL bands originating from the same defect not only for the UVL band in three GaN:Mg samples grown by HVPE, but also for the Zn-related blue band in several semi-insulating GaN:Zn samples. This interesting phenomenon can be attributed to sample nonuniformity, namely to the presence of distinct regions either in lateral or in-depth directions. We were unable to resolve these regions by scanning the sample surface with a 200-μm-diameter focused laser beam, as well as by removing 100 nm from the surface with reactive ion etching. Alternative experimental techniques, such as depth-resolved cathodoluminescence [44] or Kelvin probe microscopy [45,46], may be able to clarify the origins of these nonuniformities, which is beyond the scope of this work. It is important here that the moving UVL* band should not be confused with the BL_{Mg} band, the dominant defect-related PL band in MOCVD-grown p-type GaN:Mg, to be discussed below. The unusually large shifts of the UVL* band will be compared with the shifts of the BL_{Mg} band and explained in more detail in Sec. IV A.

D. The BL_{Mg} band in GaN:Mg grown by HVPE

The BL_{Mg} band in heavily Mg-doped GaN grown by MOCVD was extensively studied in the past [3,5–7,9,14]. In all these works, the BL_{Mg} band shifts significantly to higher photon energies with increasing excitation intensity. The BL_{Mg} band is attributed to transitions from an unknown deep donor to the shallow Mg_{Ga} acceptor. For such deep DAP-type transitions, a high concentration of at least one component (Mg in our case) is needed to cause sufficient overlap between wave functions of bound electron and hole. The BL_{Mg} band is rarely observed in MBE- and HVPE-grown GaN, probably because the deep donor is not likely to form in these growth conditions. However, we have found an HVPE-grown GaN with high concentration of Mg (sample 1840) in which the BL_{Mg} band can be observed along with the UVL band (Fig. 10). The UVL band in this sample is quickly quenched with increasing temperature from 18 to 100 K, so that at higher temperatures only the BL_{Mg} band is observed. The quenching of the UVL band is tunable by excitation intensity. For example, at $P_{exc} = 0.2$ and 100 W/cm^2, the quenching begins at critical temperatures of 100 and 130 K, respectively. The quenching of the UVL band is also abrupt, and the apparent

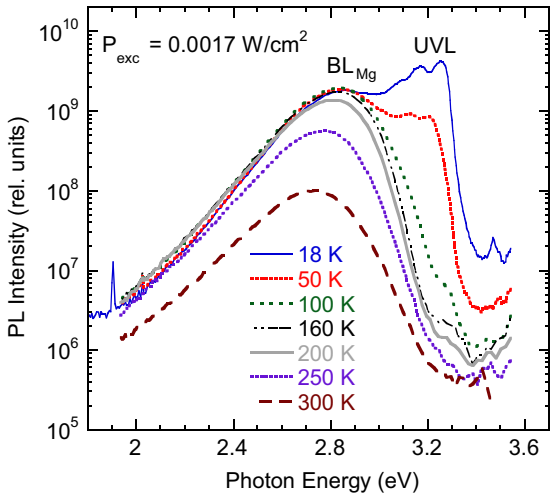

FIG. 10. Evolution of the PL spectrum with temperature for HVPE GaN:Mg, sample 1840.

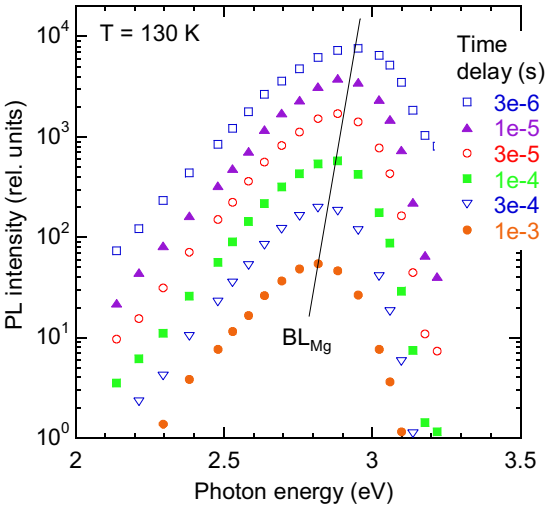

FIG. 12. Evolution of PL spectrum with time after a laser pulse at 130 K for HVPE GaN:Mg sample 1840.

"activation energy" of this quenching has no physical meaning. The BL_{Mg} band is quenched above 200 K with the activation energy of about 0.3 eV.

In contrast to the UVL* band discussed in Sec. III C, with increasing excitation intensity, the BL_{Mg} band in sample 1840 shifts to higher photon energies by only about 0.15 eV, without changing its shape (Fig. 11). The shift is about the same at temperatures between 18 and 300 K. Such shape and shift are very similar to those for the BL_{Mg} band in MOCVD-grown GaN:Mg. More detailed analysis of the shifts of the UVL* and BL_{Mg} bands will be given in Sec. IV A.

In time-resolved PL measurements, the BL_{Mg} band slowly decays after a laser pulse. The PL decay is not exponential, yet the *effective* PL lifetime could be determined by using the approach suggested in Ref. [47]. This lifetime decreases from 230 to 100 μs with increasing temperature from 130 to 220 K, and an exponential decrease of the lifetime with an activation energy of 0.34 eV is observed at higher temperatures, similar to the quenching behavior of the BL_{Mg} band intensity. The

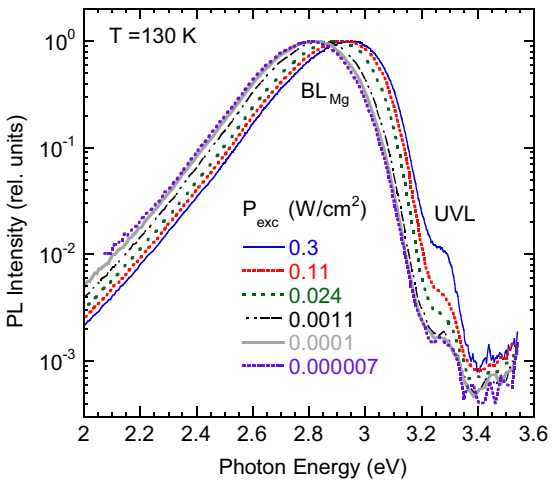

FIG. 11. Normalized PL spectra at 130 K and different excitation intensities for HVPE GaN:Mg sample 1840.

BL_{Mg} band maximum shifts to lower energies with dime delay (Fig. 12). The total shift is 0.13 eV for time delays between 3 μs and 1 ms. The slow, nonexponential decay of the BL_{Mg} intensity and the peak shift with time delay are explained with a DAP model involving a deep donor and the Mg_{Ga} acceptor [21]. The observed behavior of the BL_{Mg} band (shifts of its maximum with excitation intensity in steady-state PL and with time delay in time-resolved PL experiments, thermal quenching, and effective lifetime) is very similar to that for the BL_{Mg} band in GaN:Mg samples grown by MOCVD [6–8,21]. The fact that the UVL* band is not observed in MOCVD or HVPE GaN samples heavily doped with Mg can be explained by very high intensity of the BL_{Mg} band in these samples, dominating this part of the spectrum.

IV. DISCUSSION

A. Shifts of PL bands in GaN:Mg

Shifts of PL bands with excitation intensity are often explained with the DAP model or with a model accounting for potential fluctuations in a semiconductor with random distribution of charged impurities [7,21,48–51]. We show below that the DAP model explains the BL_{Mg} band behavior, whereas very large shifts of the UVL* band can be explained by diagonal transitions due to significant potential fluctuations or transitions in the near-surface depletion layer of GaN:Mg.

For distant DAPs, the energy of emitted photons is [49]

$$\hbar\omega(r) = E_g - E_A - E_D + E_C(r) \tag{4}$$

with

$$E_C(r) = \frac{e^2}{4\pi\varepsilon_0\varepsilon r}, \tag{5}$$

where E_g is the band gap energy, E_D and E_A are the ionization energies of the donor and acceptor, respectively, $E_C(r)$ is the Coulomb interaction between the donor and acceptor ions with separation r, e is the electron charge, ε_0 is the permittivity of vacuum, and ε is the low-frequency dielectric constant ($\varepsilon = 9.8$ for GaN [52]). The DAP emission maximum,

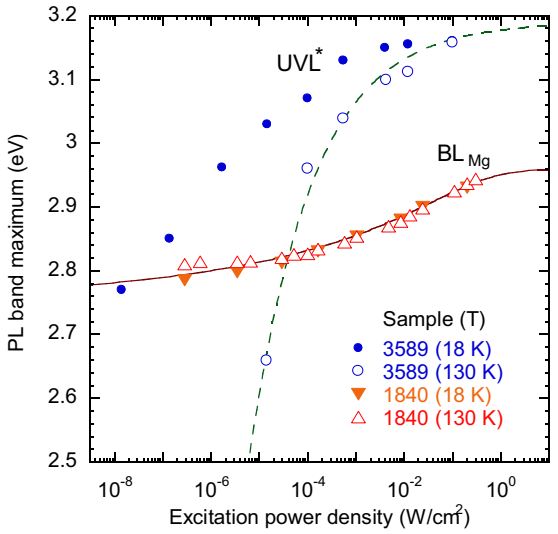

FIG. 13. Shift of PL band maxima with excitation intensity at $T = 18$ and 130 K. The BL_{Mg} band in sample 1840 and the UVL^* band in sample 3589. The solid line is calculated using Eq. (6) with $D = 100\,\mathrm{W/(eV\,cm)^2}$, $E_B = 0.48$ eV, and $\hbar\omega_\infty = 2.72$ eV. The dashed line is calculated using Eq. (9) with the following parameters: $\hbar\omega_{max} = 3.19$ eV, $N_A = 1.5 \times 10^{18}\,\mathrm{cm^{-3}}$, and $p = 3 \times 10^{19} P_{exc}[\mathrm{W/cm^2}]\,\mathrm{cm^{-3}}$.

$\hbar\omega_{max}$, corresponds to the effective Coulomb interaction $E_C = E_C(r_{eff})$. It shifts the emission peak to higher energies with increasing excitation intensity, because emission from distant pairs saturates and the contribution from close pairs with higher Coulomb interaction increases [48,49]. In the limit of infinite separations between the donor and acceptor, $\hbar\omega_\infty = E_g - E_D - E_A$.

Zacks and Halperin [53] proposed a phenomenological model, in which $\hbar\omega_{max}$, as a function of the excitation intensity P_{exc}, can be found from the following expression:

$$P_{exc} = D\frac{E_C^3}{E_B - E_C}\exp\left(-\frac{4E_B}{E_C}\right). \quad (6)$$

Here, D is a constant, $E_C = \hbar\omega_{max} - \hbar\omega_\infty$, and

$$E_B = \frac{e^2}{4\pi\varepsilon_0\varepsilon R_B} \quad (7)$$

is the Coulomb interaction energy for a pair with the separation equal to the Bohr radius R_B of a shallower component in the effective-mass approximation. The total shift of the DAP-related PL band in a very wide range of P_{exc} does not exceed $0.5E_B$ [53]. The fit of the BL_{Mg} band position with Eq. (6) is shown as a solid line in Fig. 13. According to the fit, for a noninteracting donor and acceptor (in the limit of low excitation intensity and low concentrations of donors and acceptors), the PL band maximum is expected at $\hbar\omega_\infty = 2.72$ eV. From analysis of the BL_{Mg} band shape (Fig. 11), its ZPL is shifted by $\delta = 0.15$–0.20 eV to higher energies from the BL_{Mg} band maximum (the Franck-Condon shift). Then, by taking the ionization energy of the Mg_{Ga} acceptor as $E_A = 0.2$ eV and the band gap of GaN as $E_g = 3.5$ eV, we find the ionization energy of the deep donor as $E_D = E_g - E_A - (\hbar\omega_\infty + \delta) \approx 0.4$ eV. This energy agrees with the activation energy of the BL_{Mg} band quenching (about 0.3 eV), which is attributed to thermal emission of electrons from the deep donor to the conduction band. Note that the shift of the BL_{Mg} band maximum in HVPE-grown GaN with high concentration of Mg is very similar to the shift of this band in MOCVD-grown GaN:Mg samples [3,6,7].

Now let us analyze the UVL^* band, which can be confused with the BL_{Mg} band if the PL spectrum is taken only at one excitation intensity (Figs. 5 and 6). The shift of the UVL^* band with excitation intensity is enormous, especially at elevated temperature (Fig. 13). It cannot be explained with the DAP model [43]. Indeed, according to Eq. (5), for such large shift due to the Coulomb interactions ($E_C > 0.4$–0.5 eV), the distance between the donor and acceptor of the DAP should be about 0.3 nm. For such small distances, approximations used in Eq. (4) are invalid [49]. We also notice that the average separation, r_{ave}, in the DAPs is too large in GaN:Mg sample 3589 with the Mg concentration of $N_A = 1.5 \times 10^{18}\,\mathrm{cm^{-3}}$. Indeed [54],

$$r_{ave} = (2\pi N_A)^{-1/3}, \quad (8)$$

from where $r_{ave} = 4.7$ nm. Thus, the DAP model cannot explain large shifts of the UVL^* band with excitation intensity and temperature.

However, the very large shifts of the UVL^* band can be explained in a model accounting for the potential fluctuations. Indeed, for transitions from the conduction band (or a shallow donor) to the Mg_{Ga} acceptor, the UVL band maximum depends on the potential fluctuation amplitude γ as [2,50,51]

$$\hbar\omega_m = E_g - E_A - 2\gamma, \quad (9)$$

where

$$\gamma = \frac{e^2}{4\pi\varepsilon_0\varepsilon}\frac{N_A^{2/3}}{p^{1/3}}. \quad (10)$$

The fit for the UVL^* band maximum using Eq. (9) is shown in Fig. 13 with a dashed line. We conclude that the UVL^* band is in fact the UVL band redshifted and broadened due to diagonal transitions in the semi-insulating GaN:Mg sample. The UVL^* band maximum reaches 3.16 eV at the highest excitation intensities, which is slightly lower than the energy of the UVL ZPL (~3.27 eV). However, the difference occurs because the shape of the UVL^* band does not fully convert into the UVL band shape and its maximum corresponds to the maximum of the envelope function describing contributions of LO phonon replicas to the UVL band. The two bands coexist in one sample due to its nonuniformity; i.e., areas with negligible potential fluctuations produce the UVL band, while areas with strong potential fluctuations produce the UVL^* band.

Although the fit in Fig. 13 looks very good, it should be noted that the model is simplified. In particular, at low temperatures, photogenerated charge carriers would screen potential fluctuations to the level that the height of remaining barriers for electrons and holes would not exceed several kT. This explains why the overall shift of the UVL^* band is smaller at 18 K than at 130 K (Fig. 13). Furthermore, the extremely large shifts of the UVL^* band (up to 0.6 eV at 100 K in Fig. 7) occur at temperatures and excitation intensities corresponding to abrupt and tunable quenching of PL.

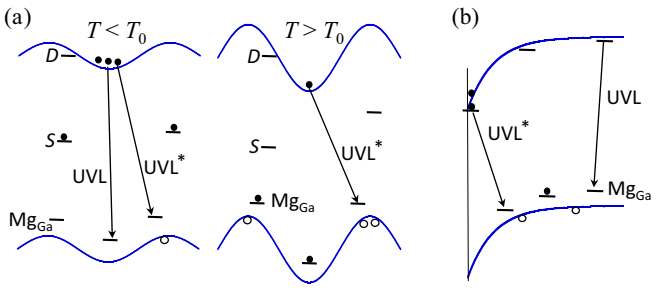

FIG. 14. Schematics of GaN bandgap and electron transitions resulting in the UVL and UVL* bands. (a) The potential fluctuations cause diagonal transitions. At $T < T_0$, nonradiative deep donors S are saturated with photogenerated electrons, and the Mg_{Ga} acceptors are saturated with holes. Under illumination, electrons accumulate in the conduction band because the nonradiative recombination channel is blocked and radiative transitions are very slow. Potential fluctuations are screened by accumulated electrons, and radiative transitions are almost vertical. At $T > T_0$, holes are emitted from the Mg_{Ga} to the valence band, the concentration of charged donors and acceptors sharply increases, while the concentration of photogenerated free electrons abruptly drops. This results in large unscreened potential fluctuations and diagonal radiative transitions. (b) The downward band bending near the sample surface causes diagonal transitions. Transitions of electrons from the conduction band (or shallow donors) at the surface to the Mg_{Ga} acceptors in the depletion region are responsible for the UVL* band, whereas such transitions in the bulk are responsible for the UVL band.

The role of the critical temperature T_0 in the energy of emitted photons is illustrated for the potential fluctuations model in Fig. 14(a). In the case of abrupt and tunable quenching of PL in semi-insulating or p-type GaN, accumulation of electrons is expected in the conduction band at low temperatures ($T < T_0$) [34]. These free electrons partially screen potential fluctuations. Additionally, deep donors become saturated with electrons, and acceptors become partially saturated with holes, even at very low excitation intensity, the so-called population inversion [34]. As a result, significantly fewer defects remain charged, which removes the origin of the potential fluctuations. Above the critical temperature ($T > T_0$), the concentration of electrons in the conduction band abruptly drops, nonradiative donors also lose bound electrons, and shallow acceptors lose bound holes, both becoming charged. These phenomena, explained with the model of abrupt and tunable quenching of PL [34], would cause potential fluctuations to rise in a narrow temperature range near T_0. The rise (and the associated shift of PL bands) is especially large at very low excitation intensities (Fig. 7) when the material becomes nearly insulating at $T > T_0$. However, at high excitation intensity, the concentration of free electrons is higher, and they partially screen the potential fluctuations. For a given concentration of free electrons, the amplitude of the potential fluctuations will increase with temperature, because the free electrons will be able to overcome higher and higher potential barriers and reduce the screening effect caused by accumulation of electrons in potential minima. This explains the large shifts of the UVL* band with temperature (at fixed excitation intensity) and with excitation intensity (at fixed temperature) at $T > T_0$ (Fig. 7).

An alternative explanation for the simultaneous observation of the UVL and UVL* bands is that the electric field causing diagonal transitions exists near the sample surface [Fig. 14(b)]. In p-type GaN, the downward band bending near the sample surface creates a barrier for free holes. At room temperature, the barrier height is about 2 eV in the dark, and it is lower than 1 eV under weak UV light [55,56]. The UVL band may originate from the region beyond the depletion region for holes, whereas the UVL* band can be attributed to recombination of electrons accumulated at the surface (in the conduction band or at shallow donors) with holes at the Mg_{Ga} acceptors located in the depletion region [Fig. 14(b)]. The behavior of PL originating from the depletion region should be similar to that from SI regions with strong potential fluctuations.

B. Attribution of PL bands in GaN:Mg

The results of this work, as well as the experimental data from numerous publications, indicate that the UVL band is caused by transitions from a shallow donor (at very low temperatures) or from the conduction band (at elevated temperatures) to the shallow Mg_{Ga} acceptor. The shape of the UVL band is typical for a shallow delocalized state with a weak electron-phonon coupling (the Huang-Rhys factor is about 0.5). The shape and the transition energy level $-/0$ of this defect at 223 ± 2 meV above the valence band maximum are the same in undoped and Mg-doped GaN samples. This finding supports the assumption that the UVL band in undoped GaN is caused by the residual Mg [35,57,58], which may originate from the Ga source. The typical concentrations of the UVL-related defect in undoped n-type GaN grown by HVPE are lower than 10^{15} cm^{-3} [35], which is below the SIMS detection limit for Mg. In n-type GaN samples (undoped or doped), the UVL band is strong because the related acceptor has a very high hole-capture coefficient ($\sim 10^{-6}$ cm^3/s) [35]. In n-type samples with the concentration of Mg close to 10^{17} cm^{-3} (sample 3590), the UVL band is the strongest defect-related band with the quantum efficiency approaching unity. No other PL bands can be found in the blue or UV region of the PL spectrum when the temperature is varied between 18 and 260 K and the UVL intensity decreases by more than three orders of magnitude (Figs. 1 and 3). Monemar *et al.* [1] previously proposed that the UVL band is caused by the Mg_{Ga}-H_i complex. However, later investigations by this group provided sufficient evidence that the UVL band is caused by the isolated Mg_{Ga} acceptor [3]. The weak localization of the hole at the Mg_{Ga} acceptor responsible for the UVL band has also been confirmed by optically detected magnetic resonance (ODMR) studies of high-purity GaN:Mg [4,59].

Our experimental results on the BL_{Mg} band with a maximum at 2.7–2.9 eV support the assumption that it is caused by electron transitions from an unknown deep donor to the shallow Mg_{Ga} acceptor [2,3,5–9,14–17]. Very high concentrations of Mg (usually close to 10^{20} cm^{-3}) are needed to observe the BL_{Mg} band, because the distances between the deep donors and the shallow Mg_{Ga} acceptors must be small enough for efficient deep DAP-type transitions. The deep donor is likely to be a complex defect involving hydrogen [3,8,16], because the BL_{Mg} band can be greatly enhanced by water vapor remote plasma treatment containing atomic hydrogen [16], and it disappears

when the hydrogen carrier gas is replaced with nitrogen during MOCVD growth [8]. In agreement with these results, the BL_{Mg} band does not appear in conductive *p*-type GaN grown by MBE, because of much lower contamination with H in this growth technique. The BL_{Mg} band also cannot be found in MOCVD-grown GaN samples where high concentrations of Mg (between 10^{19} and 10^{21} cm^{-3}) are introduced by ion implantation: only the UVL band is observed in these samples [60]. The BL_{Mg} band in heavily Mg-doped GaN should not be confused with the BL1 band (with a maximum at 2.9 eV) in undoped and Zn-doped GaN, which is associated with the Zn_{Ga} acceptor [61]. It is also different from the BL2 band (with a maximum at 3.0 eV) in high-resistivity GaN, which is assigned to the carbon-hydrogen complex [62]. The BL_{Mg} band should also be distinguished from the broadened and redshifted UVL band (UVL^* band in this study) that can exhibit very large shifts with variation of temperature or excitation intensity [18]. As was already noted by Monemar *et al.* [3], these properties of the BL_{Mg} band disagree with the predictions recently put forth by theorists for the Mg_{Ga} acceptor [26–28]. In particular, proposals on the origin of the BL_{Mg} band made in Refs. [26,27] are not supported by the experimental data. Our time-resolved PL measurements on *n*-type GaN with the concentration of Mg of 1.3×10^{17} cm^{-3} reveal a lifetime of 20 μs for the UVL band at 100 K, and no other bands could be found in the blue and UV region of the PL spectrum at time delays between 10^{-7} and 10^{-3} s. If the transition from the STS to the DGS occurred across the energy barrier ΔE, we would observe thermal quenching of the UVL band with the activation energy of ΔE with concurrent appearance of a PL band at lower photon energies, which is inconsistent with the data shown in Fig. 1. Note that the quenching of the UVL band with the activation energy of ~0.2 eV is caused by thermal emission of holes from the Mg acceptor to the valence band, which is unambiguously proven by the observation of a concurrent intensity rise for other PL bands (Fig. 3). If the DGS exists, the barrier between the STS and DGS should be larger than the Mg_{Ga} ionization energy. Moreover, in *p*-type GaN:Mg the majority of the Mg acceptors are filled with holes that should be in the DGS according to Ref. [26]. In this case, instead of the UVL band, a band from DGS should be observed at lower photon energies. However, in *p*-type GaN grown by MBE only the UVL band is observed [4,12,13]. Thus, it is unlikely that the BL_{Mg} band is caused by the isolated Mg_{Ga}.

V. CONCLUSION

The UVL band in GaN is caused by the shallow Mg_{Ga} acceptor. It is the dominant and often the only defect-related PL band in conductive *n*-type Mg-doped GaN grown by different techniques, as well as in conductive *p*-type, Mg-doped GaN grown by MBE. In GaN with the concentration of Mg exceeding 10^{19} cm^{-3}, typically grown by MOCVD and sometimes by HVPE, the BL_{Mg} band is observed at 2.7–2.9 eV. This PL band shifts with excitation intensity by up to ~0.2 eV to higher photon energies, and it is attributed to transitions from a deep donor to the shallow Mg_{Ga} acceptor. The deep donor responsible for the BL_{Mg} band is most likely a complex defect containing hydrogen. In studied semi-insulating GaN:Mg, a PL band resembling the BL_{Mg} band is in fact the UVL band redshifted and broadened due to large potential fluctuations or near-surface band bending. No experimental evidence can be found in support of a deep acceptor state, which is sometimes proposed to explain the blue band in GaN:Mg. Thus, from the experimental point of view, the Mg_{Ga} in GaN is a shallow acceptor with delocalized wave function. The extensive experimental data on Mg in GaN indicate that the hole is weakly localized at the Mg_{Ga} acceptor, which raises a question why the dual nature of the Mg acceptor is not observed in experiment.

ACKNOWLEDGMENTS

The work was supported by the National Science Foundation (DMR-1410125). The authors thank Jacob Leach from Kyma Technologies, Inc., Alex Usikov from Nitride Crystals, Inc., and Raffaella Calarco from Paul-Drude Institute (Berlin, Germany) for the GaN:Mg samples used in this work.

APPENDIX: SOLUTION OF RATE EQUATIONS FOR *n*- AND *p*-TYPE GaN:Mg

The complex behavior of PL in Mg-doped GaN with variation of temperature and excitation intensity, as well as the wide range of PL lifetimes reported but not explained in the literature, becomes more apparent if we derive approximate analytical expressions by using a simple phenomenological model. Three major types of defects should be included to describe adequately the kinetics of PL in GaN: a shallow donor *D*, a radiative acceptor *A* (the shallow Mg_{Ga} acceptor in our case), and the dominant nonradiative recombination center *S* (Fig. 15) [34]. This nonradiative center can be a deep donor or a deep acceptor. The exciton or near-band-edge (NBE) emission can be ignored in the first approximation, because it is weak.

The rate equations describing flows of electrons and holes (when the *S* center is a deep acceptor) can be written down from transitions shown in Fig. 15 as

$$\frac{\partial n}{\partial t} = G - C_{nA}N_A^0 n - C_{nS}N_S^0 n - C_{nD}N_D^+ n + N_D^0 Q_D, \tag{A1}$$

$$\frac{\partial p}{\partial t} = G - C_{pA}N_A^- p - C_{pS}N_S^- p + N_A^0 Q_A, \tag{A2}$$

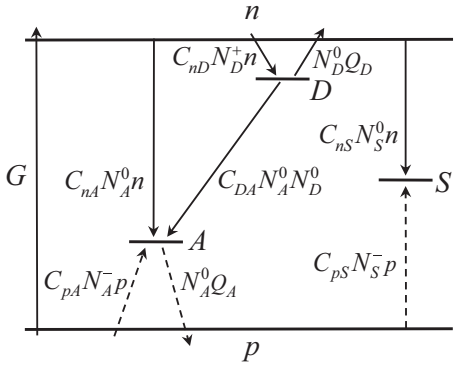

FIG. 15. Band diagram of GaN:Mg. The solid arrows show transitions of electrons, and the dashed arrows show transitions of holes. *A* is the Mg_{Ga} acceptor, *D* is a shallow donor, and *S* is a nonradiative deep acceptor. Model parameters are defined in the text.

TABLE II. Parameters of the samples.

Parameter	n type (sample 3590)	p type (sample 9599A)	p type (sample 9600A)
C_{DA} (cm^3/s)	10^{-13}	2.5×10^{-12}	2.5×10^{-12}
C_{nA} (cm^3/s)	3.2×10^{-12}	3.2×10^{-12}	3.2×10^{-12}
C_{pA} (cm^3/s)	0.5×10^{-6}	0.5×10^{-6}	0.5×10^{-6}
C_{nS} (cm^3/s)	3×10^{-6}	3×10^{-6}	3×10^{-6}
C_{pS} (cm^3/s)	10^{-6}	10^{-6}	10^{-6}
C_{nD} (cm^3/s)	10^{-8}	10^{-8}	10^{-8}
B (cm^3/s)	3×10^{-11}	3×10^{-11}	3×10^{-11}
N_D (cm^{-3})	2.5×10^{17}	10^{17}	10^{17}
N_A (cm^{-3})	1.3×10^{17}	4.9×10^{19}	2.3×10^{19}
N_S (cm^{-3})	4×10^{16}	10^{18}	10^{18}
E_D (meV)	15	20	20
E_A (meV)	185	150	150

$$\frac{\partial N_D^0}{\partial t} = C_{nD} N_D^+ n - C_{DA} N_D^0 N_A^0 - N_D^0 Q_D, \tag{A3}$$

$$\frac{\partial N_S^0}{\partial t} = C_{pS} N_S^- p - C_{nS} N_S^0 n, \tag{A4}$$

$$\frac{\partial N_A^0}{\partial t} = C_{pA} N_A^- p - C_{nA} N_A^0 n - C_{DA} N_A^0 N_D^0 - N_A^0 Q_A. \tag{A5}$$

Here, C_{nA}, C_{nD}, and C_{nS} are electron-capture coefficients for A, D, and S centers, respectively; C_{pA} and C_{pS} are hole-capture coefficients for A and S centers; C_{DA} is the effective coefficient of DAP recombination; n and p are the concentrations of free electrons and holes, respectively; N_A^0, N_A^-, N_D^0, N_D^+, N_S^0, and N_S^- are the concentrations of A, D, and S centers in different charge states. When the S center is a deep donor, N_S^0 and N_S^- should be replaced with N_S^+ and N_S^0, respectively. Thermal emission coefficients for electrons at shallow donors and for holes at the Mg_{Ga} acceptors are

$$Q_D = C_{nD} N_c g^{-1} \exp(-E_D/kT) \tag{A6}$$

and

$$Q_A = C_{pA} N_v g^{-1} \exp(-E_A/kT), \tag{A7}$$

respectively. Here, E_D and E_A are the ionization energies of the shallow donor and the Mg_{Ga} acceptor, respectively, g is the degeneracy factor of the donor and acceptor levels (assumed to be equal to 2 for both), and N_c and N_v are the effective densities of states in the conduction and valence bands, respectively ($N_c = 5 \times 10^{14} T^{3/2}$ cm^{-3} and $N_v = 3.2 \times 10^{15} T^{3/2}$ cm^{-3} for GaN) [34]. Equations (A1) and (A2) describe the rates of change of the free electron and free hole concentrations, respectively; Eq. (A3) describes the gain and loss of electrons by the shallow donors; Eqs. (A4) and (A5) describe the gain and loss of holes by the nonradiative centers S and Mg_{Ga} acceptors, respectively. For steady-state conditions, all derivatives are equal to zero. The charge neutrality requires that

$$p + N_D^+ = n + N_A^- + N_S^-, \tag{A8}$$

if the S center is a deep acceptor, and

$$p + N_D^+ + N_S^+ = n + N_A^-, \tag{A9}$$

if the S center is a deep donor.

The parameters of the model for three samples (n- and p-type GaN:Mg) are given in Table II. The C_{nA} and C_{pA} for the shallow acceptor in GaN are equal or close to the previously reported parameters [2,30]. The activation energy for the Mg_{Ga} acceptor in lightly Mg-doped GaN is found from thermal quenching of the UVL band (Sec. III A), and that in heavily Mg-doped GaN is found from the temperature-dependent Hall effect on samples with similar doping [63,64]. $E_D \approx 15-20$ meV for GaN with the concentration of shallow donors between 2×10^{16} and 3×10^{17} cm^{-3} (Ref. [30]). The values of $N_A = [\mathrm{Mg}]$ are found from SIMS measurements (Table I), and the concentrations of D and S centers are chosen as the most reasonable expectations. The C_{DA} parameter is expected to be about the same order of magnitude as the C_{nA} parameter [50]. However, it decreases with increasing DAP separations, that are larger in the lightly Mg-doped GaN sample. The parameters C_{nD}, C_{nS}, and C_{pS} are close to previously found parameters for defects in GaN [31,34]. They also agree with typical nonradiative recombination and capture parameters reported in the literature. The highest electron- and hole-capture coefficients in different semiconductors are observed for attractive centers (donors for electrons and acceptors for holes) and are in the range of 10^{-7} to 10^{-5} cm^3/s for temperatures between 20 and 200 K [65–67].

Figure 16 shows the temperature dependence of free electrons in n-type GaN:Mg (sample 3590) and that of free holes in p-type GaN:Mg (sample 9600A) in the dark, calculated by using the following expressions [68]:

$$\frac{n(n + N_A + N_S)}{N_D - N_A - N_S - n} = \frac{N_c}{g} \exp\left(-\frac{E_D}{kT}\right), \tag{A10}$$

$$\frac{p(p + N_D)}{N_A - N_D - p} = \frac{N_v}{g} \exp\left(-\frac{E_A}{kT}\right), \tag{A11}$$

with parameters from Table II. With these parameters, the concentration of free electrons at 100 K is 1.5×10^{16} cm^{-3} in sample 3590, and the concentrations of free holes at 295 K are 1×10^{18} and 6×10^{17} cm^{-3} in samples 9599A and 9600A,

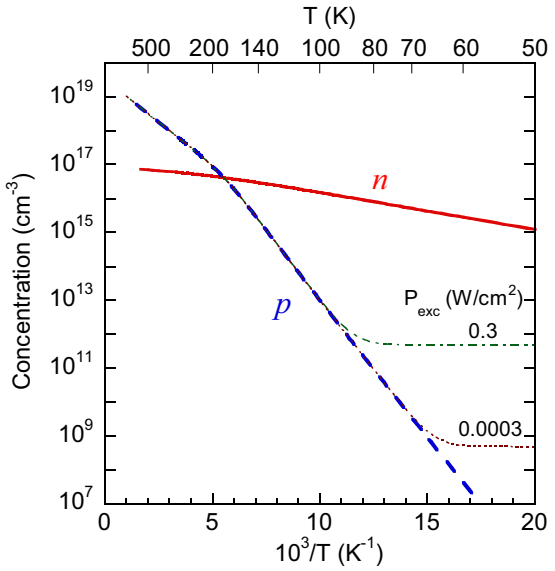

FIG. 16. Temperature dependences of the concentrations of free electrons in n-type GaN:Mg (sample 3590) and free holes in p-type GaN:Mg (sample 9600A). The thick solid curve for n is calculated using Eq. (A10). The thick dashed curve for p is calculated using Eq. (A11). The thin dash-dotted and dotted curves for p are from numerical solutions of Eqs. (A1)–(A9) for $P_{\rm exc} = 0.3$ and 0.0003 W/cm^2, respectively. The parameters are given in Table II.

respectively. All these values agree with the experimentally found values shown in Table I. Below, we derive analytical expressions for the case of low excitation intensity when PL intensity from defects is not saturated. To satisfy this condition, the electron-hole generation rate $G = 10^{20}$ cm^{-3} s^{-1} is chosen. It corresponds to the excitation power density of about 0.001 W/cm^2. Three cases will be considered: (a) conductive n type, (b) conductive p type, and (c) semi-insulating material.

1. *n*-type GaN:Mg

In n-type GaN:Mg, the Fermi level is close to the shallow donor level. At low excitation intensity, the defect states below the Fermi level are mostly filled with electrons, so that $N_A^0 \ll N_A^- \approx N_A$, $N_S^0 \ll N_S^- \approx N_S$, $N_D^+ \approx N_S + N_A$, and $N_D^0 \approx N_D - N_S - N_A$. For $T > 50$ K, the thermal (dark) concentration of electrons greatly exceeds the concentration of optically generated electrons ($n_{\rm opt} \approx 10^{11}$ cm^{-3} for $G = 10^{20}$ cm^{-3} s^{-1}). With these approximations, Eqs. (A1)–(A5) for steady-state conditions become linear and can be solved. It is convenient to introduce characteristic times that illustrate a competition between different processes: $\tau_{pA} = (C_{pA}N_A)^{-1} = 1.5 \times 10^{-11}$ s and $\tau_{pS} = (C_{pS}N_S)^{-1} = 8.3 \times 10^{-12}$ s (both independent of temperature if C_{pA} and C_{pS} are constant); $\tau_{nD} = (C_{nD}n)^{-1} = 6.7 \times 10^{-9}$ s, $\tau_{nA} = (C_{nA}n)^{-1} = 2 \times 10^{-5}$ s, $\tau_{DA} = (C_{DA}N_D^0)^{-1} = 1.3 \times 10^{-4}$ s, and $\tau_{nS} = (C_{nS}n)^{-1} = 2.2 \times 10^{-11}$ s (all at 100 K when $n = 1.5 \times 10^{16}$ cm^{-3}).

For example, τ_{nA} is the lifetime of the UVL band in n-type GaN. Indeed, the rate of electron transitions from the conduction band to the acceptor A can be presented as $I_{e-A}^{\rm UVL} = C_{nA}N_A^0 n = n/\tau_{nA}$. For temperatures below PL quenching, the last term in Eq. (A5) can be ignored, and the equation can be written as

$$\frac{\partial N_A^0}{\partial t} = \frac{p}{\tau_{pA}} - \frac{N_A^0}{\tau_{nA}} - \frac{N_A^0}{\tau_{DA}}. \tag{A12}$$

With $\tau_{pA} \ll \tau_{nA}, \tau_{DA}$, the solution of Eq. (A12) for $t \gg \tau_{pA}$ is $N_A^0(t) = N_A^0(0)\exp(-t/\tau_0)$ [42], where $\tau_0^{-1} = \tau_{nA}^{-1} + \tau_{DA}^{-1}$. In fact, the decay of the DAP emission is nonexponential and appears as a long tail of the (e-A) component, if these components cannot be spectrally resolved. When the (e-A) component has the largest contribution, the decay is nearly exponential: $I_{e-A}^{\rm UVL}(t) = I_{e-A}^{\rm UVL}(0)\exp(-t/\tau_{nA})$. This lifetime, $\tau_0 \approx \tau_{nA}$, experimentally determined from time-resolved PL measurements, allows finding the concentration of free electrons and its temperature dependence $n(T)$, when the electron-capture coefficient C_{nA} is known [30].

Time constants τ_{pA} and τ_{pS} are the characteristic times of capture of photogenerated holes by A and S centers, respectively. For temperatures below PL quenching, the last term in Eq. (A2) can be neglected, and Eq. (A2) becomes

$$\frac{\partial p}{\partial t} = G - \frac{p}{\tau_{pA}} - \frac{p}{\tau_{pS}}. \tag{A13}$$

After a laser pulse ($G = 0$ at $t > 0$), the concentration of free holes decays as $p(t) = p(0)\exp(-t/\tau_p)$, where $\tau_p = (\tau_{pA}^{-1} + \tau_{pS}^{-1})^{-1} \approx 1 \times 10^{-11}$ s. The UVL quantum efficiency, $\eta_{\rm UVL} = I^{\rm UVL}/G = p/(\tau_{pA}G)$, is independent of temperature and is governed by the capture rate of holes. From Eq. (A13) for steady-state conditions ($\partial p/\partial t = 0$), we have

$$\eta_{\rm UVL} = \frac{\frac{p}{\tau_{pA}}}{\frac{p}{\tau_{pA}} + \frac{p}{\tau_{pS}}} = \frac{\tau_{pS}}{\tau_{pA} + \tau_{pS}} = 0.6. \tag{A14}$$

We also find for steady-state conditions from Eq. (A13) with $G = 10^{20}$ cm^{-3} s^{-1} that $p = G\tau_p = 1 \times 10^9$ cm^{-3}. With this p, we find that $N_S^0 \approx 10^9$ cm^{-3} from Eq. (A4) and $N_A^0 \approx 10^{15}$ cm^{-3} from Eq. (A5). These estimates justify approximations made above.

At temperatures above 130 K, thermal emission of holes from the Mg_{Ga} acceptor to the valence band becomes substantial, and its rate eventually becomes nearly equal to the rate of hole capture by this acceptor ($p/\tau_{pA} \approx N_A^0 Q_A$). N_A^0 decreases as $\propto \exp(E_A/kT)$ and Q_A increases as $\propto \exp(-E_A/kT)$ with temperature. The critical temperature T_A, at which the thermal quenching of the UVL band begins, can be found from the condition $\tau_0 = \tau_{\rm therm}$, where τ_0 is PL lifetime and $\tau_{\rm therm}$ is the characteristic time of thermal emission of holes from the A center, defined in Eq. (3). Then,

$$T_A = \frac{E_A}{k\ln[\tau_{nA}(1-\eta_0)C_{pA}g^{-1}N_v]} \approx 130 \text{ K}. \tag{A15}$$

In a wide range of temperatures (50–300 K), the UVL quantum efficiency and its lifetime have the following temperature dependencies [42]:

$$\eta(T) = \frac{\eta_0}{1 + \tau_0/\tau_{\rm therm}}, \tag{A16}$$

$$\tau(T) = \frac{\tau_0}{1 + \tau_0/\tau_{\rm therm}}, \tag{A17}$$

where $\tau_{\text{therm}}^{-1} = (1-\eta_0)Q_A$ and $\tau_0 \approx \tau_{nA} = (C_{nA}n)^{-1}$. Equation (A16) is identical to Eqs. (1)–(3). At $T > T_A$, the *measured* PL lifetime decreases with temperature as $\tau(T) \propto \exp(E_A/kT)$ and is equal to the thermal emission time ($\tau \approx \tau_{\text{therm}}$), whereas *actual* PL lifetime (τ_0) remains unchanged. The important difference between measured and actual PL lifetimes is discussed in Ref. [42]. When the UVL band is quenched, other PL bands rise due to competition for holes between different recombination channels [34,40]. In particular, the RL band intensity changes with temperature as [33]

$$I^{\text{RL}}(T) = I^{\text{RL}}(0)\frac{1-\frac{I^{\text{UVL}}(T)}{I^{\text{UVL}}(0)}\eta_0}{1-\eta_0}, \tag{A18}$$

where $I^{\text{RL}}(T)$, $I^{\text{UVL}}(T)$, $I^{\text{RL}}(0)$, and $I^{\text{UVL}}(0)$ are intensities of the RL and UVL bands at arbitrary temperature and in the limit of low temperatures, respectively. From the best fit of the $I^{\text{RL}}(T)$ dependence for sample 3590 (Fig. 3) we find $\eta_0 = 0.7$ for the UVL band.

The above model reproduces the behavior of the UVL band in *n*-type GaN:Mg. In particular, the UVL intensity is independent of temperature up to $T_A \approx 130$ K, and it decreases with an activation energy of $E_A = 185$ meV at $T > T_A$ (Figs. 1 and 3). Intensities of other PL bands rise concurrently with the quenching of the UVL band. The UVL lifetime, measured with time-resolved PL, is 20 μs at $T < T_A$, and it decreases exponentially with the activation energy close to E_A at $T > T_A$.

2. *p*-type GaN:Mg

In *p*-type GaN:Mg, the Fermi level is close to the Mg_{Ga} acceptor level, not far from the valence band. In a wide range of temperatures ($T > 100$ K), the thermal concentration of holes (in dark) is higher than the concentration of optically generated holes (for $G = 10^{20}$ cm^{-3} s^{-1}). In this case, recombination channels compete for electrons as minority charge carriers. The dominant nonradiative recombination center S is a deep acceptor, with high capture cross section for both holes and electrons (see parameters in Table II). As will be demonstrated in next section, the experimental results for conductive *p*-type GaN:Mg can be explained on the assumption that the dominant nonradiative defect is a deep acceptor, not a donor.

At low excitation intensity, the defect states above the Fermi level are mostly empty, so that $N_S^- \ll N_S^0 \approx N_S$, $N_D^0 \ll N_D^+ \approx N_D$, $N_A^- \approx N_D$, and $N_A^0 \approx N_A - N_D$. The N_D^0 and N_S^- are small and they depend on T and G, while the $p(T)$ dependence for $T > 100$ K is known (Fig. 16). The characteristic times of transitions in this case are the following: $\tau_{nD} = (C_{nD}N_D)^{-1} = 10^{-9}$ s, $\tau_{nS} = (C_{nS}N_S)^{-1} = 3.3 \times 10^{-13}$ s, $\tau_{nA} = (C_{nA}N_A^0)^{-1} = 1.4 \times 10^{-8}$ s, $\tau_{DA} = (C_{DA}N_A^0)^{-1} = 1.7 \times 10^{-8}$ s, and $\tau_{pA} = (C_{pA}N_A^-)^{-1} = 2 \times 10^{-11}$ s. In particular, very short hole-capture characteristic time in Mg-doped GaN ($\tau_{pA} \approx 1 \times 10^{-11}$s) was confirmed by direct femtosecond pump-probe technique measurements [69].

At very low temperatures, the last term in Eq. (A1) can be ignored, with the result

$$\frac{\partial n}{\partial t} = G - \frac{n}{\tau_n}, \tag{A19}$$

where τ_n is the characteristic time of escape of photogenerated electrons from the conduction band and $\tau_n^{-1} = \tau_{nA}^{-1} + \tau_{nS}^{-1} + \tau_{nD}^{-1} \approx \tau_{nS}^{-1}$. In steady-state conditions, $n = G\tau_n \approx 3 \times 10^7$ cm^{-3}. This concentration is independent of temperature, because it is dominated by the temperature-independent term τ_{nS}.

At very low temperatures, the DAP-type transitions dominate over the (e-A)-type transitions in the UVL band, because the nonradiative capture of free electrons by shallow donors is much faster than the radiative recombination via the Mg_{Ga} acceptor ($\tau_{nD} \ll \tau_{nA}$) and thermal emission of electrons from the shallow donors is too slow compared to the DAP recombination time ($\tau_{DA} \ll Q_D^{-1}$). Above a critical temperature, T_D, which can be found from the condition $\tau_{DA} = Q_D^{-1}$ as

$$T_D = \frac{E_D}{k\ln[\tau_{DA}C_{nD}g^{-1}N_c]} \approx 75 \text{ K}, \tag{A20}$$

the DAP mechanism yields to the e-A mechanism for the UVL band. At $T \gg T_D$, $N_D^0 Q_D \gg C_{DA}N_D^0 N_A^0$ in Eq. (A3), with the result

$$C_{nD}N_D^+ n = N_D^0 Q_D, \tag{A21}$$

where $N_D^0 \ll N_D^+ \approx N_D$. By expressing N_D^0 from Eq. (A21) and taking $n = 3 \times 10^7$ cm^{-3} and $N_D = 10^{17}$ cm^{-3}, we can find the quantum efficiency of the UVL band at $T > 100$ K:

$$\eta^{\text{UVL}}(T) = \frac{C_{nA}N_A^0 n + C_{DA}N_A^0 N_D^0}{G} = \frac{C_{nA}N_A^0 n}{G}\left[1 + \frac{C_{DA}}{C_{nA}}\frac{N_D g}{N_c}\exp(E_D/kT)\right]. \tag{A22}$$

For the chosen parameters of the model, $\eta^{\text{UVL}}(100\ K) = 9.2 \times 10^{-5}$, $\eta^{\text{UVL}}(200\ K) = 3.0 \times 10^{-5}$, and $\eta^{\text{UVL}}(300\ K) = 2.5 \times 10^{-5}$ (compare with data for sample 9600A in Fig. 3). With further increase of temperature, the η^{UVL} does not change. The quantum efficiency of the UVL band is orders of magnitude lower than that of the nonradiative recombination, because minority carriers (both optically generated and thermally emitted electrons) are captured much faster by nonradiative S centers than by the Mg_{Ga} acceptors ($\tau_{nS} \ll \tau_{nA}$).

In time-resolved PL measurements, after a laser pulse ($G = 0$ at $t > 0$), photogenerated electrons very quickly escape from the conduction band to all available defects as $n(t) = n(0)\exp(-t/\tau_n)$, where $\tau_n \approx 3 \times 10^{-13}$ s. At very low temperature, DAP-type recombination with relatively fast decay ($\tau_{DA} \approx 2 \times 10^{-8}$ s) may have significant contribution to the PL decay and cause fast and *nonexponential* decay. With increasing temperature, when $\tau_{DA} > Q_A^{-1}$, the majority of photogenerated electrons would be redirected to the fast nonradiative recombination channel. The observed decay of the UVL will be very fast in this case, close to the exponential decay with $\tau_{nS} \approx 3 \times 10^{-13}$ s. These predictions for conductive *p*-type GaN:Mg agree with experimentally observed very fast PL decay (subnanosecond) [19].

At $T > T_A$, where $T_A \approx 170$ K from Eq. (A15), the capture and emission rates for holes at acceptor A become nearly equal

$(C_{pA}N_A^- p \approx N_A^0 Q_A)$, and we find that

$$p \approx \frac{N_A^0 Q_A}{C_{pA}N_A^-} = \frac{(N_A - N_D)N_v}{N_D g}\exp(-E_A/kT). \quad \text{(A23)}$$

At these temperatures, the intensity of the NBE emission (exciton or band-to-band transitions) increases as $\propto \exp(-E_A/kT)$ because it is proportional to the product of the hole and electron concentrations, and the latter is independent of temperature at $T > T_A$. In Fig. 3, the temperature dependence of the NBE emission intensity is shown with the thick dashed line. The NBE emission efficiency is calculated as $\eta_{NBE} = Bnp/G$, where n and p are obtained from numerical solutions of Eqs. (A1)–(A9) for sample 9600A and $B = 3 \times 10^{-11}$ cm^3/s, which agrees with the reported radiative recombination coefficients for GaN [70,71]. Such rise in the NBE intensity with temperature can be observed only for conductive p-type GaN:Mg, where the Fermi level is close to the Mg_{Ga} acceptor level, and $N_A^0 \approx N_A$. Thus, it can serve as a proof of p-type conductivity when the Hall effect measurements are inconclusive or cannot be done.

The model reproduces the behavior of the UVL band in conductive p-type GaN:Mg at $T > 100$ K. In particular, the UVL intensity decreases with very low activation energy as temperature increases up to $T \approx 200$ K and it saturates at higher temperatures (Fig. 3). The UVL quantum efficiency is very low, much lower than that for n-type GaN:Mg. The UVL lifetime, measured with time-resolved PL, is shorter than 10 ns (temporal resolution of our time-resolved PL system). The NBE emission rises with temperature in agreement with increasing concentration of free holes.

Analysis of rate equations for p-type GaN:Mg at temperatures *below* 100 K or at arbitrary excitation intensity is complicated due to nonlinearity of Eqs. (A1)–(A5). In these conditions, interesting phenomena may occur, such as population inversion and abrupt and tunable quenching of PL.

3. Abrupt and tunable quenching of PL in GaN:Mg

The experimental data for sample 9600A in a wider range of temperatures are compared with numerical solutions of Eqs. (A1)–(A9) in Fig. 17. The temperature dependence of the quantum efficiency of the UVL band is very weak, and it is the same at low and high excitation intensity. Interestingly, theoretical curves are nearly identical at $T > 100$ K, but very different at $T < 100$ K for two cases: when the S center is a deep acceptor and when it is a deep donor. Only for the first case, the calculations agree with experiment in entire range of temperatures, which indicates that the dominant nonradiative defect in MBE-grown p-type GaN samples is a *deep acceptor*. It may look surprising that the C_{nS} for the deep nonradiative acceptor is so large ($C_{nS} = 3 \times 10^{-6}$ cm^3/s), because a neutral acceptor is not expected to capture electrons efficiently. However, as was shown by Alkauskas *et al.* [72], this apparent controversy can be resolved with the assumption that the dominant nonradiative defect has an excited state which quickly captures electrons. Note that the calculated $\eta(T)$ dependence is very sensitive to the value of C_{nS}, but not sensitive at all to the value of C_{pS} (between 10^{-10} and 10^{-4} cm^3/s) for the case when the S center is a deep acceptor.

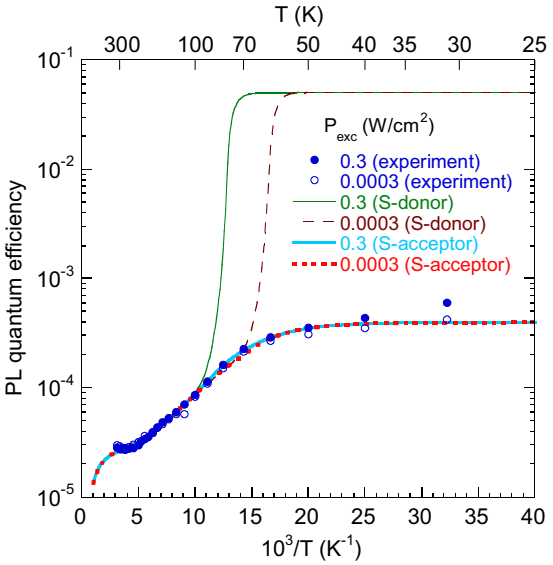

FIG. 17. Temperature dependence of the quantum efficiency of the UVL band in p-type GaN:Mg. The symbols are experimental data for sample 9600A at $P_{exc} = 0.0003$ and 0.3 W/cm^2. The lines are calculated using Eqs. (A1)–(A9) with parameters listed in Table II. Thick dotted and solid lines are calculated for the case of S center as a deep acceptor, and thin dashed and solid lines are calculated for the case of S center as a deep donor.

However, when the dominant nonradiative center is a deep donor, abrupt and tunable quenching of PL is always observed, if parameters of the model are varied within reasonable ranges. This phenomenon is explained by saturation of the dominant nonradiative center with photogenerated electrons and the ensuing blockade of this recombination channel at low temperatures [34]. The blockade also results in increased concentration of electrons in the conduction band and inversion of the conductivity from p type to n type under illumination. Indeed, from Eqs. (A1) and (A2), when the nonradiative recombination and thermal emission are ignored, the following relations are obtained:

$$C_{pA}N_D p = C_{nA}(N_A - N_D)n \approx G. \quad \text{(A24)}$$

From Eq. (A24), we find $n = 1.4 \times 10^{12}$ cm^{-3} and $p = 2 \times 10^9$ cm^{-3} for $G = 10^{20}$ cm^{-3} s^{-1} and other parameters taken from Table II for sample 9600A. At $T > T_0$, n abruptly drops and the conductivity reverts to p type. It appears that in semi-insulating GaN:Mg samples grown by HVPE the dominant nonradiative defect is a *deep donor*. This would explain the very high quantum efficiency of the UVL and UVL* bands and the abrupt and tunable quenching of PL for sample 3589 (Sec. III C).

The dramatic difference between the PL behaviors in these two cases (Fig. 17) is unexpected, because all the parameters are identical except for the type of the dominant nonradiative center. To explain this result, below we derive analytical expressions for low temperatures and low excitation intensities. These results demonstrate that the crucial difference between these two cases is the degree of saturation of S centers with electrons under illumination.

In the limit of low temperature and low excitation intensity, $n, p \ll N_A, N_D, N_S$, $C_{nA} N_A^0 n \approx 0$, $N_D^0 Q_D \approx 0$, and $N_A^0 Q_A \approx 0$ in Eqs. (A1)–(A9). It is also expected for p-type GaN:Mg that $N_A > N_S > N_D$. Then, analytical expressions for all variables can be found. To avoid cumbersome formulas [73], we present here results for the practical case of $\alpha = \frac{C_{pS}}{C_{pA}} \frac{C_{nD}}{C_{nS}} \ll 1$ ($\alpha \approx 0.007$ for parameters of p-type GaN:Mg in Table II and $\alpha = 2 \times 10^{-6}$ for parameters used for calculated curves on Fig. 8).

When the S center is a deep acceptor, $N_A^- \approx \alpha N^*$, $N_A^0 \approx N_A - \alpha N^*$, $N_S^- \approx N_D - \alpha N^*$, $N_S^0 \approx N_S - N_D + \alpha N^*$, $N_D^0 \approx G\alpha N^* C_{pA} (C_{DA} C_{pS} N_A N_D)^{-1}$, $N_D^+ \approx N_D$, $p \approx G(C_{pS} N_D)^{-1}$, and $n \approx G\alpha N^* C_{pA} (C_{pS} C_{nD})^{-1} N_D^{-2}$, where $N^* = N_D^2 (N_S - N_D)^{-1}$. In these conditions, S centers are not saturated with electrons ($N_S^0 = 0.90 N_S$ for parameters used in Fig. 17 and $N_S^0 = 0.375 N_S$ for parameters in Fig. 8), recombination of photogenerated electrons and holes occurs mostly via these nonradiative centers, and the UVL quantum efficiency is very weak.

When the S center is a deep donor, $N_A^- \approx N_D + \alpha N_S$, $N_A^0 \approx N_A - N_D - \alpha N_S$, $N_S^0 \approx (1 - \alpha) N_S$, $N_S^+ \approx \alpha N_S$, $N_D^0 \approx G(C_{DA} N_A)^{-1}$, $N_D^+ \approx N_D$, $n \approx G(C_{nD} N_D)^{-1}$, and $p \approx G(C_{pS} N_S + C_{pA} N_D)^{-1}$. In this case, S centers are saturated with electrons, even in the limit of low excitation intensity ($N_S^0 = 0.993 N_S$ for parameters used in Fig. 17 and $N_S^0 = 0.999998 N_S$ for parameters in Fig. 8), the nonradiative recombination channel is blocked, and the UVL efficiency is high. The population inversion is observed in this case, and nonradiative donors are saturated with electrons. This quasiequilibrium condition occurs due to specific relation between capture coefficients, namely $\alpha \ll 1$.

[1] B. Monemar, P. P. Paskov, G. Pozina, C. Hemmingsson, J. P. Bergman, T. Kawashima, H. Amano, I. Akasaki, T. Paskova, S. Figge, D. Hommel, and A. Usui, Phys. Rev. Lett. **102**, 235501 (2009).

[2] M. A. Reshchikov and H. Morkoç, J. Appl. Phys. **97**, 061301 (2005).

[3] B. Monemar, P. P. Paskov, G. Pozina, C. Hemmingsson, J. P. Bergman, S. Khromov, V. N. Izyumskaya, V. Avrutin, X. Li, H. Morkoç, H. Amano, M. Iwaya, and I. Akasaki, J. Appl. Phys. **115**, 053507 (2014).

[4] E. R. Glaser, M. Murthy, J. A. Freitas, Jr., D. F. Storm, L. Zhou, and D. J. Smith, Physica B **401-402**, 327 (2007).

[5] L. Eckey, V. von Gfug, J. Holst, A. Hoffmann, A. Kaschner, H. Siegle, C. Thomsen, B. Schineller, K. Heime, M. Heuken, O. Schön, and R. Beccard, J. Appl. Phys. **84**, 5828 (1998).

[6] U. Kaufmann, M. Kunzer, M. Maier, H. Obloh, A. Ramakrishnan, and B. Santic, Appl. Phys. Lett. **72**, 1326 (1998).

[7] M. A. Reshchikov, G.-C. Yi, and B. W. Wessels, Phys. Rev. B **59**, 13176 (1999).

[8] F. Shahedipour and B. W. Wessels, Appl. Phys. Lett. **76**, 3011 (2000).

[9] L. S. Wang, W. K. Fong, C. Surya, K. W. Cheah, W. H. Zheng, and Z. G. Wang, Solid State Electron. **45**, 1153 (2001).

[10] E. R. Glaser, T. A. Kennedy, J. A. Freitas, Jr., B. V. Shanabrook, A. E. Wickenden, D. D. Koleske, R. L. Henry, and H. Obloh, Physica B **273-274**, 58 (1999).

[11] M. S. Brandt, N. M. Johnson, R. J. Molnar, R. Singh, and T. D. Moustakas, Appl. Phys. Lett. **64**, 2264 (1994).

[12] M. A. L. Johnson, Z. Yu, C. Boney, W. C. Hughes, J. W. Cook Jr., J. F. Schetzina, H. Zhao, B. J. Skromme, and J. A. Edmund, Mater. Res. Soc. Symp. Proc. **449**, 215 (1997).

[13] A. M. Fischer, S. Wang, F. A. Ponce, B. P. Gunning, C. A. M. Fabien, and W. A. Doolitle, Phys. Status Solidi B **254**, 1600668 (2017).

[14] U. Kaufmann, M. Kunzer, H. Obloh, M. Maier, Ch. Manz, A. Ramakrishnan, and B. Santic, Phys. Rev. B **59**, 5561 (1999).

[15] H. Alves, M. Böhm, A. Hofstaetter, H. Amano, S. Einfeldt, D. Hommel, D. M. Hofmann, and B. K. Meyer, Physica B: Condens. Matter **308**, 38 (2001).

[16] Y. Kamiura, M. Kaneshiro, J. Tamura, T. Ishiyama, Y. Yamashita, T. Mitani, and T. Mukai, Jpn. J. Appl. Phys. **44**, L926 (2005).

[17] Y. Koide, D. E. Walker, Jr., B. D. White, L. J. Brillson, M. Murakami, S. Kamiyama, H. Amano, and I. Akasaki, J. Appl. Phys. **92**, 3657 (2002).

[18] E. Oh, H. Park, and Y. Park, Appl. Phys. Lett. **72**, 70 (1998).

[19] M. Smith, G. D. Chen, J. Y. Lin, H. X. Jiang, A. Salvador, B. N. Sverdlov, A. Botchkarev, H. Morkoç, and B. Goldenberg, Appl. Phys. Lett. **68**, 1883 (1996).

[20] A. L. Gurskii, I. P. Marko, E. V. Lutsenko, V. N. Pavlovskii, V. Z. Zubialevich, G. P. Yablonskii, B. Schineller, O. Schön, and M. Heuken, Phys. Status Solidi B **228**, 361 (2001).

[21] F. Shahedipour and B. W. Wessels, MRS Internet J. Nitride Semicond. Res. **6**, 12 (2001).

[22] M. Godlewski, T. Suski, I. Grzegory, S. Porowski, J. P. Bergman, W. M. Chen, and B. Monemar, Physica B **273-274**, 39 (1999).

[23] H. Teisseyre, B. Kozankiewicz, M. Leszczynski, I. Grzegory, T. Suski, M. Bockowski, S. Porowski, K. Pakula, P. M. Mensz, and I. B. Bhat, Phys. Status Solidi B **198**, 235 (1996).

[24] C. G. Van de Walle and J. Neugebauer, J. Appl. Phys. **95**, 3851 (2004).

[25] C. G. Van de Walle, S. Limpijumnong, and J. Neugebauer, Phys. Rev. B **63**, 245205 (2001).

[26] S. Lany and A. Zunger, Appl. Phys. Lett. **96**, 142114 (2010).

[27] J. L. Lyons, A. Janotti, and C. G. Van de Walle, Phys. Rev. Lett. **108**, 156403 (2012).

[28] G. Miceli and A. Pasquarello, Phys. Rev. B **93**, 165207 (2016).

[29] D. O. Demchenko, I. C. Diallo, and M. A. Reshchikov, Phys. Rev. B **97**, 205205 (2018).

[30] M. A. Reshchikov, J. D. McNamara, M. Toporkov, V. Avrutin, H. Morkoç, A. Usikov, H. Helava, and Yu. Makarov, Sci. Rep. **6**, 37511 (2016).

[31] M. A. Reshchikov, J. D. McNamara, S. Fernández-Garrido, and R. Calarco, Phys. Rev. B **87**, 115205 (2013).

[32] M. A. Reshchikov, D. O. Demchenko, J. D. McNamara, S. Fernández-Garrido, and R. Calarco, Phys. Rev. B **90**, 035207 (2014).

[33] M. A. Reshchikov, M. A. Foussekis, J. D. McNamara, A. Behrends, A. Bakin, and A. Waag, J. Appl. Phys. **111**, 073106 (2012).
[34] M. A. Reshchikov, A. A. Kvasov, M. F. Bishop, T. McMullen, A. Usikov, V. Soukhoveev, and V. A. Dmitriev, Phys. Rev. B **84**, 075212 (2011).
[35] M. A. Reshchikov, A. Usikov, H. Helava, Yu. Makarov, V. Prozheeva, I. Makkonen, F. Tuomisto, J. H. Leach, and K. Udwary, Sci. Rep. **7**, 9297 (2017).
[36] M. A. Reshchikov, J. D. McNamara, F. Zhang, M. Monavarian, A. Usikov, H. Helava, Yu. Makarov, and H. Morkoç, Phys. Rev. B **94**, 035201 (2016).
[37] B. J. Skromme and G. L. Martinez, MRS Internet J. Nitride Semicond. Res. **5S1**, W9.8 (2000).
[38] J. L. Lyons, A. Janotti, and C. G. Van de Walle, Appl. Phys. Lett. **97**, 152108 (2010).
[39] M. Matsubara and E. Bellotti, J. Appl. Phys. **121**, 195702 (2017).
[40] M. A. Reshchikov and R. Y. Korotkov, Phys. Rev. B **64**, 115205 (2001).
[41] The stepwise rise of the YL1 band with increasing temperature from 100 to 160 K is almost identical to that of the RL band (by a factor of 3). However, the effect is veiled by a decrease of the YL1 band intensity with temperature, which is evident at temperatures above 150 K.
[42] M. A. Reshchikov, J. Appl. Phys. **115**, 103503 (2014).
[43] P. Ghimire, Study of the photoluminescence spectra of Mg-doped GaN, M.S. thesis, Virginia Commonwealth University, 2017.
[44] L. J. Brillson, J. Phys. D: Appl. Phys. **45**, 183001 (2012).
[45] R. Bozek, K. Pakula, and J. M. Baranowski, Phys. Status Solidi C **1**, 364 (2004).
[46] B. Han, B. W. Wessels, and M. P. Ulmer, J. Appl. Phys. **98**, 023513 (2005).
[47] R. Y. Korotkov, M. A. Reshchikov, and B. W. Wessels, Physica B **325**, 1 (2003).
[48] F. E. Williams, J. Phys. Chem. Solids **12**, 265 (1960).
[49] D. G. Thomas, M. Gershenzon, and F. A. Trumbore, Phys. Rev. **133**, A269 (1964).
[50] A. P. Levanyuk and V. V. Osipov, Sov. Phys. Usp. **24**, 187 (1981).
[51] B. I. Shklovskii and A. L. Efros, *Electronic Properties of Doped Semiconductors* (Springer, Berlin, 1984), pp. 53–73 and 253–313.
[52] W. J. Moore, J. A. Freitas, Jr., and R. J. Molnar, Phys. Rev. B **56**, 12073 (1997).
[53] E. Zacks and A. Halperin, Phys. Rev. B **6**, 3072 (1972).
[54] F. Williams, Phys. Status Solidi **25**, 493 (1968).
[55] J. P. Long and V. M. Bermudez, Phys. Rev. B **66**, 121308 (2002).
[56] M. Foussekis, J. D. McNamara, A. A. Baski, and M. A. Reshchikov, Appl. Phys. Lett. **101**, 082104 (2012).
[57] B. Monemar, P. P. Paskov, T. Paskova, J. P. Bergman, G. Pozina, W. M. Chen, P. N. Hai, I. A. Buyanova, H. Amano, and I. Akasaki, Mater. Sci. Eng., B **93**, 112 (2002).
[58] S. Khromov, C. Hemmingsson, B. Monemar, L. Hultman, and G. Pozina, J. Appl. Phys. **116**, 223503 (2014).
[59] M. E. Zvanut, J. Dashdorj, J. A. Freitas, E. R. Glaser, W. R. Willoughby, J. H. Leach, and K. Udwary, J. Electron. Mater. **45**, 2692 (2016).
[60] H. Tsuge, K. Ikeda, S. Kato, T. Nishimura, T. Nakamura, K. Kuriyama, and T. Mishima, Nucl. Instrum. Methods Phys. Res., Sect. B **409**, 50 (2017).
[61] D. O. Demchenko and M. A. Reshchikov, Phys. Rev. B **88**, 115204 (2013).
[62] D. O. Demchenko, I. C. Diallo, and M. A. Reshchikov, J. Appl. Phys. **119**, 035702 (2016).
[63] T. Tanaka, A. Watanabe, H. Amano, Y. Kobayashi, I. Akasaki, S. Yamazaki, and M. Koike, Appl. Phys. Lett. **65**, 593 (1994).
[64] W. Gotz, R. S. Kern, C. H. Chen, H. Liu, D. A. Steigerwald, and R. M. Fletcher, Mater. Sci. Eng., B **59**, 211 (1999).
[65] M. Lax, J. Phys. Chem. Solids **8**, 66 (1959).
[66] V. N. Abakumov, V. I. Perel, and I. N. Yassievich, *Nonradiative Recombination in Semiconductors* (Elsevier, Amsterdam, 1991), pp. 88–97.
[67] K. D. Glinchuk, K. Lukat, and V. E. Rodionov, Fiz. Tekh. Poluprovodn. (S. Peterburg) **15**, 1337 (1981) [Sov Phys. Semicond. **15**, 772 (1981)].
[68] G. L. Pearson and J. Bardeen, Phys. Rev. **75**, 865 (1949).
[69] K.-H. Lin, G.-W. Chern, S.-W. Chu, C.-K. Sun, H. Xing, Y. Smorchkova, S. Keller, U. Mishra, and S. P. DenBaars, Appl. Phys. Lett. **81**, 3975 (2002).
[70] A. Dmitriev and A. Oruzheinikov, J. Appl. Phys. **86**, 3241 (1999).
[71] J. S. Im, A. Moritz, F. Steuber, V. Härle, F. Scholz, and A. Hangleiter, Appl. Phys. Lett. **70**, 631 (1997).
[72] A. Alkauskas, C. E. Dreyer, J. L. Lyons, and C. G. Van de Walle, Phys. Rev. B **93**, 201304 (2016).
[73] M. A. Reshchikov, Phys. Rev. B **85**, 245203 (2012).